# Changes in peripapillary and macular vascular measured using optical coherence tomography angiography after glaucoma drainage device procedures

Doctoral thesis

to obtain a doctorate (Dr. med.)

from the Faculty of Medicine

of the University of Bonn

**Siqi Fan**

from Shandong/China

2026

Written with authorization of

the Faculty of Medicine of the University of Bonn

First reviewer: Prof. Dr. Frank G. Holz

Second reviewer: Prof. Dr. MUDr. Valentin S. Schäfer

Day of oral examination: 14.01.2026

From the Clinic and Polyclinic for the Eye Clinic of University of Bonn

# Table of contents

## List of abbreviations

| | |
|---|---|
| IOP | Intraocular Pressure |
| AGV | Ahmed Glaucoma Valve |
| BCVA | Best Corrected Visual Acuity |
| BGI | Baerveldt Glaucoma Implant |
| CDI | Color Doppler Imaging |
| CDR | Cup-to-Disc Ratio |
| dVD | deep Vascular Density |
| ETDRS | Early Treatment Diabetic Retinopathy Study |
| FAZ | Foveal Avascular Zone |
| FFA | Fundus Fluorescein Angiography |
| GAT | Goldmann Applanation Tonometer |
| GDD | Glaucoma Drainage Device |
| ICGA | Indocyanine Green Angiography |
| IN | Inferior Nasal |
| IN | Inferior Nasal |
| IT | Inferior Temporal |
| IT | Inferior Temporal |
| LDF | Laser Doppler Flowmetry |
| LSFG | Laser Speckle Flowgraphy |
| MD | Mean Deviation |
| MIGS | Minimally Invasive Glaucoma Surgeries |
| mRNFL | macular Retinal Nerve Fiber Layer |
| OCT | Optical Coherence Tomography |
| OCTA | Optical Coherence Tomography Angiography |
| ONH | Optic Nerve Head |
| OPP | Ocular Perfusion Pressure |
| PACG | Primary Angle-Closure Glaucoma |
| PGI | Paul® Glaucoma Implant |
| POAG | Primary Open-Angle Glaucoma |

| | |
|---|---|
| pRNFL | peripapillary Retinal Nerve Fiber Layer |
| PSD | Pattern Standard Deviation |
| RGC | Retinal Ganglion Cells |
| RPC | Radial Peripapillary Capillaries |
| RPE | Retinal Pigment Epithelium |
| SD | Standard Deviation |
| SD-OCT | Spectral Domain OCT |
| SN | Superior Nasal |
| SN | Superior Nasal |
| SS-OCT | Swept-Source OCT |
| ST | Superior Temporal |
| ST | Superior Temporal |
| sVD | superficial Vascular Density |
| VD | Vascular Density |
| VF | Visual Field |
| VFI | Visual Field Index |

# 1 Introduction

Glaucoma is one of the leading causes of irreversible blindness worldwide, significantly affecting patients' visual health and overall quality of life (Jonas et al., 2017). While intraocular pressure (IOP) remains a central factor in the pathophysiology and progression of glaucoma, there is increasing interest and ongoing debate regarding the potential contribution of retrobulbar blood flow to the disease process (Nuzzi et al., 2018).

## 1.1 What is Glaucoma

Glaucoma is a group of diseases that damage the optic nerve and its visual pathways, characterized by optic nerve head (ONH) cupping and visual field (VF) defects (Gupta et al., 2006; Nuzzi et al., 2018; Jonas et al., 2017). It is primarily associated with pathologically elevated IOP and is one of the leading causes of irreversible blindness worldwide.(Nuzzi et al., 2018; Klugah-Brown et al., 2024; Davis et al., 2016). The main pathological mechanism of glaucoma is typically related to increased IOP, and numerous large clinical studies have shown that elevated IOP remains the only modifiable risk factor (Jayaram et al., 2023). However, the pathophysiology of glaucoma is multifactorial, and its occurrence and progression are not solely limited to increased IOP. In addition to elevated IOP, genetic susceptibility and age-related changes also play significant roles in the disease process (Zukerman et al., 2020; Wiggs und Pasquale, 2017). Genetic factors may make individuals more susceptible to glaucoma, affecting the structure and function of the optic nerve or altering the body's response to changes in IOP (van Koolwijk et al., 2012). Furthermore, age is a well-recognized risk factor, and the incidence and severity of glaucoma tend to increase with age (Bell et al., 2020; Caprioli, 2013). This may be related to age-related changes in ocular structures and function, including reduced aqueous humor outflow and vascular changes affecting the ONH (Zhang et al., 2021).

### 1.1.1 Pathogenesis of Glaucoma

The pathogenesis of glaucoma remains unclear. Two main theories have been proposed: the mechanical compression theory and the vascular ischemia theory (Flammer, 1994; Fechtner und Weinreb, 1994). The mechanical compression theory attributes

glaucomatous damage to elevated IOP, which compresses intraocular structures and the optic disc. This pressure deforms and displaces the lamina cribrosa, disrupting axoplasmic flow in nerve fibers and causing transport blockages at the lamina cribrosa level (Quigley et al., 1981). Animal studies have also confirmed that elevated IOP impairs axoplasmic transport, affects axonal protein production and transport, disrupts the normal metabolism of retinal ganglion cells (RGCs), and ultimately induces apoptosis (Quigley und Addicks, 1980). This theory emphasizes the direct compressive damage to the optic nerve caused by elevated IOP. Although studies have confirmed that elevated IOP is an independent risk factor for glaucoma, it cannot fully explain the onset and progression of all glaucoma cases.

The vascular ischemia theory postulates that glaucomatous optic neuropathy is secondary to insufficient ocular blood perfusion. This insufficiency may be associated with elevated IOP or other systemic conditions, such as hypertension, vascular spasms, or diabetes, which affect local ocular blood flow (Di Zhao et al., 2014; Mitchell et al., 1997). Reduced ocular perfusion leads to vascular dysregulation, causing localized hypoxia and oxidative stress responses. These processes increase the levels of matrix metalloproteinases and endothelin-1, triggering RGC apoptosis and tissue remodeling (Ko et al., 2005; Emre et al., 2005; Tezel, 2006).

Understanding these multifactorial mechanisms is crucial for formulating comprehensive management and treatment strategies aimed at protecting vision and improving the quality of life for patients with glaucoma.

Disease Classification

Glaucoma can be classified in various ways based on etiology, anatomy, and pathogenesis. Clinically, it is commonly divided into three main categories: primary glaucoma, secondary glaucoma, and congenital glaucoma.

Primary glaucoma includes two major subtypes: open-angle glaucoma and angle-closure glaucoma. Primary open-angle glaucoma (POAG) is the most common type, characterized by chronic blockage or dysfunction of the trabecular meshwork, leading to impaired aqueous humor outflow and gradually increasing IOP (Gedde et al., 2021; Weinreb und Khaw, 2004; Weinreb et al., 2016). This condition usually progresses without

obvious symptoms and often results in gradual and irreversible vision loss by the time it is detected (Jonas et al., 2017). On the other hand, primary angle-closure glaucoma (PACG) occurs when the peripheral iris mechanically blocks the anterior chamber angle due to an existing iris configuration, leading to impaired aqueous humor drainage (Sun et al., 2017).

Secondary glaucoma refers to glaucoma caused by other ocular or systemic diseases. Its pathophysiology is driven by the interference of normal aqueous humor circulation due to certain ocular or systemic conditions or the improper use of specific medications. Common primary causes of secondary glaucoma include inflammation, trauma, hemorrhage, vascular diseases, medications, ocular surgeries, and space-occupying lesions in the eye (Li et al., 2024; Camp et al., 2019; Tang et al., 2023; Ahmad et al., 2023). In these cases, increased IOP results from underlying pathologies that either obstruct aqueous humor outflow or increase aqueous humor production, ultimately causing optic nerve damage.

Congenital glaucoma is a type of glaucoma caused by abnormal development of the anterior chamber structures during embryonic and developmental stages of eye formation, with most cases present at birth (Ko et al., 2015; deLuise und Anderson, 1983; Luntz, 1979). Histopathologically, there are three types of developmental abnormalities: trabeculodysgenesis, iridotrabeculodysgenesis, and corneotrabeculodysgenesis (Sihota et al., 2024). The comprehensive theory regarding the mechanism of congenital glaucoma suggests that the development of the anterior chamber angle is hindered due to disruption of the neural crest cell-derived process, resulting in abnormal development of the trabecular meshwork, forward attachment of the ciliary body and iris to the trabecular meshwork, and abnormalities in Schlemm’s canal (Kupfer und Kaiser-Kupfer, 1979; Williams et al., 2017; García-Antón et al., 2017). These mechanisms, alone or in combination, lead to increased resistance to aqueous humor outflow. Up to 40 % of congenital glaucoma are familial and follow autosomal recessive inheritance patterns with variable penetrance (Lewis et al., 2017; Ho und Walton, 2004).

### 1.1.2 Epidemiology

According to global eye health research, glaucoma is the second leading cause of blindness after cataracts (Flaxman et al., 2017). However, unlike cataracts, vision loss

caused by glaucoma is irreversible. As of 2023, it is estimated that over 80 million people worldwide are affected by glaucoma, and this number is projected to exceed 110 million by 2040 (Allison et al.; Tham et al., 2014). This increase is primarily attributed to the aging global population, along with the rising prevalence of risk factors such as elevated IOP, family history, and other lifestyle-related factors (Zhang et al., 2021; Thomas et al., 2015).

### 1.1.3 The Importance of Treatment

Currently, there is no treatment available to restore vision lost due to glaucoma, making case detection and effective treatment crucial. With an aging population, the prevalence of glaucoma is expected to rise significantly in the coming decades (Jayaram et al., 2023). While glaucoma cannot be fully cured, early detection and timely intervention can significantly slow disease progression and preserve remaining visual function (Heijl et al., 2002; Francesco et al., 2024).

At present, lowering IOP remains the cornerstone of glaucoma treatment, encompassing medical therapy, laser procedures, and surgical interventions. It is essential to emphasize that reducing IOP is the only proven method for treating glaucoma (Jonas et al., 2017). By effectively managing IOP, we can prevent or delay irreversible optic nerve damage and vision loss. Since glaucoma often progresses in its early stages without noticeable symptoms, early intervention through regular screening and timely treatment is critical to safeguarding vision and maintaining a good quality of life (Musa et al., 2022).

## 1.2 The Role of Vascular Factors in Glaucoma

### 1.2.1 Structure and Function of the Retina

The retina is a highly specialized neural tissue located at the posterior pole of the eye, with its primary function being the conversion of light signals into neural signals, which are transmitted to the brain via the optic nerve to form vision. Structurally, the retina comprises two distinct layers: the outer retinal pigment epithelium (RPE) and the inner neurosensory retina (Yuan et al., 2024).

The fovea centralis is a specialized region located at the posterior pole of the retina, characterized by the absence of retinal vasculature in its central area, known as the foveal avascular zone (FAZ). This unique anatomical feature endows the fovea with

exceptionally high spatial resolution and color discrimination. The optic disc, located approximately 3 mm nasal to the fovea, is a well-demarcated, orange-red, circular structure where the optic nerve exits the globe. The central retinal artery and vein traverse the optic disc, with their branches supplying the retinal layers (D'Amico, 1994).

The retina is characterized by a high metabolic rate. This elevated metabolic activity is evidenced by the continuous shedding of photoreceptor outer segments, which require ongoing phagocytosis and metabolism by the RPE. Additionally, the retina's rich vascular supply underscores its high metabolic demand. The retina relies on the central retinal vascular system and the ciliary vascular system, which form four distinct capillary networks: the radial peripapillary capillary plexus on the surface of the nerve fiber layer, the superficial and deep capillary plexuses within the inner nuclear layer, and the choriocapillaris (Wright et al., 2020). Disruption of the microcirculation can lead to localized hypoxia, triggering degenerative changes in RGCs.

### 1.2.2 Effects of Glaucoma on Retinal Vasculature

The primary pathological changes in glaucoma are characterized by optic nerve damage and VF defects. Studies have demonstrated that vascular factors play a significant role in the progression of the disease (Moraes et al., 2012; Harris et al., 2005; Cantor et al., 2018). Elevated IOP is hypothesized to exert mechanical compression on the vasculature, thereby reducing the perfusion pressure of the ONH and retina, leading to insufficient blood flow and increasing the risk of optic nerve damage (Sigal und Ethier, 2009; Resch et al., 2011). Additionally, the autoregulatory capacity of blood vessels in glaucoma patients is often impaired, limiting their ability to adjust blood flow in response to fluctuating demands, thereby heightening the risk of ischemia (Luo et al., 2015; Weigert et al., 2005). Furthermore, retinal microcirculatory abnormalities associated with glaucoma may result in disrupted oxygen metabolism, which exacerbates neural damage (Nguyen et al., 2022; Olafsdottir et al., 2014).

In this context, retinal vascular density (VD) has emerged as a critical parameter for assessing the status of retinal microcirculation. VD reflects the integrity and functionality of the retinal vascular network and serves as an indirect marker of perfusion and metabolic health.

Research has found that the VD in glaucoma patients significantly decreases and is closely associated with both structural damage to the optic nerve and functional VF defects. Additionally, some studies have suggested that baseline retinal capillary density may help predict the structural progression of glaucoma (Verticchio Vercellin et al., 2024).

The study of VD using Optical Coherence Tomography Angiography (OCTA) has provided important insights into the vascular components of glaucoma pathophysiology, highlighting the necessity of utilizing advanced imaging technologies and analytical tools to further investigate their role in disease progression and treatment response.

## 1.3 Old Imaging and New Imaging

### 1.3.1 Historical Developments and Early Imaging Modalities

In the past few decades, significant progress has been made in the study of retinal vascular factors in glaucoma research. Techniques such as Color Doppler Imaging (CDI), Laser Doppler Flowmetry (LDF), and Laser Speckle Flowgraphy (LSFG), which began in the late 1980s, have become essential tools for exploring the vascular factors involved in glaucoma (Matthiessen et al., 2004; Sehi, 2011; Garcia et al., 2002; Briers und Fercher, 1982).

This technology has revealed the characteristics of retrobulbar blood flow in glaucoma patients, demonstrating a higher resistivity index and lower flow velocity compared to healthy individuals (Hamard et al., 1994; Rankin et al., 1996). It underscores the role of vascular factors in disease progression. Other imaging techniques, such as Fundus Fluorescein Angiography (FFA) and Indocyanine Green Angiography (ICGA), have also been employed in the study of the optic disc, retinal, and choroidal vascular structures (François und Laey, 1974; Hayreh, 1972; Staurenghi et al., 2005).

Despite the contributions of early imaging technologies, they faced several inherent challenges. For instance, the use of contrast agents or the need for pupil dilation increased patient risk and discomfort, while limited resolution hindered the capture of fine details in the retinal capillary network. Furthermore, these techniques required high patient cooperation, which limited their practical application. Meanwhile, technologies such as

CDI primarily measured blood flow velocity and resistance, rather than providing structural information on vascular density.

With technological advancements, imaging methods have gradually shifted towards non-invasive, high-resolution approaches. Optical Coherence Tomography (OCT), introduced in the 1990s, laid the foundation for retinal structural imaging (Nij Bijvank et al., 2023). Subsequently, the advent of OCTA overcame many limitations of earlier methods, enabling non-invasive, quantitative, and layered visualization of retinal vasculature (Bazvand et al., 2017).

These technological advances have not only deepened our understanding of glaucoma-related microvascular changes but also emphasized the importance of continually improving imaging techniques to integrate structural and functional metrics, thereby better elucidating the relationship between vascular changes and glaucoma damage.

### 1.3.2 Advancements with OCTA

OCTA is a relatively recent technology based on the principles of OCT. It captures detailed images of retinal and choroidal blood flow by detecting the motion contrast of red blood cells within the vessels. OCTA distinguishes between static tissue and flowing blood by performing multiple scans of the same retinal area (Spaide et al., 2018; Carlo et al., 2015).

The development of this technology has been facilitated by advances in both hardware and software. For instance, the introduction of Spectral Domain OCT (SD-OCT) enhanced imaging speed and resolution, while Swept-Source OCT (SS-OCT) provided greater tissue penetration (Kashani et al., 2017). Additionally, motion detection and artifact elimination have improved the reliability and accuracy of vascular imaging (Cicinelli et al., 2018). Unlike earlier imaging methods that required invasive techniques or contrast agents, OCTA offers a fully non-invasive, high-resolution alternative capable of visualizing microvascular structures at the capillary level.

The unique advantages of OCTA have established it as a critical tool in both clinical and research settings. OCTA enables quantitative analysis of metrics such as VD and perfusion area, facilitating the assessment of vascular changes in glaucoma and other diseases. Its rapid scanning time minimizes patient discomfort, while its non-invasive

nature eliminates the risks associated with dye injection, thereby broadening its applicability (Maram et al., 2017; Kashani et al., 2017).

In glaucoma research, OCTA is particularly valuable for its ability to visualize and quantify microvascular changes. Studies have demonstrated that OCTA can detect reduced vascular density in the peripapillary and macular regions of glaucomatous eyes, even in the early stages of the disease (Mannil et al., 2023; Chang et al., 2021). These findings suggest that OCTA could serve as a complement to traditional structural OCT metrics, such as retinal nerve fiber layer thickness, providing a more comprehensive approach to the diagnosis and monitoring of glaucoma.

## 1.4 Surgical Management

The primary goal of glaucoma treatment is to reduce IOP to slow or prevent further damage to the optic nerve. Currently, treatment modalities for glaucoma include pharmacological therapy, laser procedures, and surgical intervention. When medication and laser treatments prove insufficient or when the disease progresses rapidly, surgical management is typically employed (Stein et al., 2021).

### 1.4.1 Classification of Surgical Procedures and the Use of Glaucoma Drainage Devices

Surgical management of glaucoma can be broadly categorized into several types. Traditional filtering surgeries, such as trabeculectomy, effectively lower IOP by creating an external drainage pathway for aqueous humor (Nouri-Mahdavi et al., 1995). Minimally invasive glaucoma surgeries (MIGS), such as the iStent and Xen, involve smaller surgical incisions, allowing for faster postoperative recovery, but are generally suitable only for specific indications (Fellman et al., 2020). Glaucoma drainage devices (GDDs), such as the Ahmed glaucoma valve (New World Medical Inc, Rancho Cucamonga, CA) and the Baerveldt glaucoma implant (Advanced Medical Optics, Santa Ana, CA), function by implanting a drainage tube within the eye to divert aqueous humor to the posterior subconjunctival space for absorption (Lim, 2022; Poelman et al., 2020).

The Ahmed glaucoma valve (AGV) and the Baerveldt glaucoma implant (BGI) are the most commonly used and extensively studied GDDs. Both devices consist of a hollow silicone tube with an internal lumen diameter exceeding 300 microns, facilitating the

drainage of aqueous humor from the anterior chamber to an external implant plate located beneath the conjunctiva, where fluid absorption occurs (Coleman et al., 1995). The AGV incorporates a Venturi-type valve mechanism to prevent early postoperative hypotony, whereas the BGI lacks a valve and instead requires an internal stent and/or external ligature to regulate fluid outflow and prevent hypotony.

### 1.4.2 PAUL glaucoma implant

Traditional glaucoma drainage devices, such as the AGV and BGI, have demonstrated efficacy in clinical practice but are not without limitations. For instance, the unidirectional valve mechanism of AGV can lead to postoperative IOP spikes, while BGI, lacking a unidirectional valve, requires closer postoperative monitoring of IOP fluctuations to prevent hypotony (Budenz et al., 2015; Christakis et al., 2017; Budenz et al., 2011). To address these shortcomings, the Paul® glaucoma implant (Advanced Ophthalmic Innovations, Singapore, Republic of Singapore) was developed as a safer and more efficient alternative.

The Paul® glaucoma implant (PGI) is a valveless drainage device made of medical-grade silicone. Compared to traditional implants, the PGI features a larger plate surface area (342 mm²), significantly greater than that of the AGV (184 mm²) and slightly smaller than the BGI (350 mm²), with a design that reduces the portions of the external implant plate obscured by the extraocular muscles. Additionally, the PGI incorporates a smaller lumen diameter (127µm), which is intended to mitigate early postoperative hypotony and theoretically reduce the risk of corneal endothelial damage (Khodeiry und Sayed, 2023; Koh et al., 2020).

The PGI demonstrates enhanced anatomical compatibility compared to conventional drainage devices, making it suitable for a wide range of glaucoma patients. Its soft, low-irritation material minimizes tissue irritation and scar formation post-implantation, thereby reducing complications associated with traditional devices. Through these innovations, the PGI offers a safe and effective alternative for the surgical management of glaucoma.

## 1.5 Aim of study

Although studies have investigated changes in retinal VD in glaucoma patients following anti-glaucoma surgeries, particularly through the use of OCTA to evaluate retinal vascular alterations, no research to date has specifically examined the outcomes associated with PGI. Specifically, it remains unclear whether retinal VD increases following such procedures.

The primary objective of this study is to utilize OCTA to evaluate changes in vascular density around the optic nerve head and macular regions in glaucoma patients undergoing PGI. This research aims to address a gap in the existing literature by providing data that enhance understanding of the potential impact of PGI surgery on retinal microcirculation and vascular health. Furthermore, it seeks to explore the role of this procedure in preserving or restoring visual function in glaucoma patients.

# 2 Materials and methods

## 2.1 Subjects

### 2.1.1 Patient Enrollment

This prospective study included 20 glaucoma patients who underwent PGI surgery at the Department of Ophthalmology, Bonn University Hospital, between April 2023 and July 2024. Patients were enrolled into the database at the time of surgery, and follow-up data were collected at each postoperative visit. All analyses were performed using a de-identified dataset. The study was approved by the local ethics committee of Bonn University Hospital. The study protocol adhered to the ethical guidelines of the 2000 Declaration of Helsinki and received prior approval from the institution's Human Research Committee.

*Inclusion criteria:* Patients aged between 21 and 80 years, diagnosed with glaucoma, and who had an IOP that remained uncontrolled despite maximum tolerated medical therapy. The study included patients with primary glaucoma, regardless of whether they had previously undergone failed trabeculectomy, aqueous shunt implantation, or other intraocular surgeries. Secondary glaucoma patients were also included, such as those with neovascular glaucoma, uveitic glaucoma, traumatic glaucoma, aphakic glaucoma, or glaucoma associated with iris-corneal endothelial syndrome.

*Exclusion criteria:* Factors that could affect the quality of imaging, such as severe cataracts or media opacities in the cornea or vitreous, were excluded from the study.

### 2.1.2 Examination Instruments

In this study, all patients underwent a comprehensive and systematic ophthalmic examination both preoperatively and during follow-up, utilizing a variety of standardized diagnostic instruments to ensure data accuracy and comparability. The specific diagnostic equipment and their applications were as follows:

Uncorrected visual acuity and Best Corrected Visual Acuity (BCVA) were assessed using a standardized Snellen chart, with visual acuity results converted to logMAR values for

statistical analysis. IOP was measured using a Goldmann Applanation Tonometer (GAT). Patient demographic information, glaucoma type, prior surgical history, and current antiglaucoma medication usage (type and dosage) were collected through the electronic medical record system.

The anterior segment structures, including the conjunctiva, cornea, anterior chamber, iris, and lens, were thoroughly examined using a slit lamp (e.g., Haag-Streit or equivalent equipment) to assess the presence of any preoperative or postoperative complications. The anterior chamber angle was evaluated using a three-mirror or four-mirror gonioscope (e.g., Goldmann or Sussman lens) under the slit lamp, with a focus on angle openness and pigment deposition, to assist in diagnosing glaucoma types, particularly angle-closure or mixed glaucomas.

Functional optic nerve damage was assessed using the Humphrey Field Analyzer (Carl Zeiss Meditec, Inc., Dublin, CA) with the standard 24-2 automated static VF test. Structural imaging of the macula and optic disc regions was performed using the Heidelberg HRA+OCT Spectralis system to measure macular retinal nerve fiber layer (mRNFL) thickness, peripapillary retinal nerve fiber layer (pRNFL) thickness, and other parameters, aiding in the assessment of glaucomatous optic neuropathy.

VD images of the optic disc, peripapillary region, and macular area were obtained using the Zeiss Plex Elite 9000 device. Key parameters measured included superficial vascular density (sVD), deep vascular density (dVD), and the area and perimeter of the FAZ, with the aim of quantifying microcirculatory changes and exploring their correlation with IOP, visual field, and OCT parameters.

All examinations were conducted by trained technicians or ophthalmologists following standardized protocols to enhance data quality and consistency.

### 2.1.3 Definition of Glaucoma

Glaucomatous ONH changes were defined by the presence of diffuse or focal thinning of the neuroretinal rim, optic disc rim defects, or a vertical cup-to-disc ratio difference of $\geqslant$ 0.2 between the two eyes. VF test results were consistent with glaucoma characteristics, with the presence of $\geqslant$3 abnormal clusters of non-edge points on the pattern deviation

map, each having a probability lower than 5 % of the normal population, with at least one point having a probability lower than 1 %. Additionally, the pattern standard deviation (PSD) p-value was <5 %, or the Glaucoma Hemifield Test showed "outside normal limits" on two preoperative VF tests (Kourkoutas et al., 2014; Chakravarti, 2017), with confirmation by two glaucoma specialists (K.M. and M.P.).

### 2.1.4 Indications for PGI Surgery

The PGI surgery is indicated for patients with inadequate IOP control despite maximum tolerated medical therapy and/or failure of filtering glaucoma surgeries. It can also serve as the primary surgical option in certain high-risk patients for filtering surgery failure (Oatts und Han, 2023). Its application is not limited to POAG but also includes various types of secondary glaucoma, such as neovascular glaucoma, uveitic glaucoma, aphakic glaucoma, congenital glaucoma, and glaucoma associated with iris-corneal endothelial syndrome (Ramdas et al., 2019; Stallworth et al., 2023; Pakravan et al., 2007; Walkden und Au, 2018). Additionally, in cases with conjunctival scarring, such as those previously treated with vitrectomy, retinal buckle surgery, silicone oil tamponade, or filtering surgery failure, PGI offers a more reliable alternative due to the reduced success rate of filtering surgeries (Gedde et al., 2021; Vries et al., 2016). Studies have shown that, compared to repeat trabeculectomy, GDD surgeries such as PGI implantation have a higher success rate and a lower incidence of complications (Gedde et al., 2012). Furthermore, in patients with conjunctival scarring, traditional filtering surgeries, which rely on healthy conjunctiva, are prone to failure, making GDD a superior treatment option due to its lower dependence on conjunctival health and lower risk of scarring (Almousa und Lake, 2014). The indications for aqueous humor drainage tubes are expanding, and these devices are increasingly used in surgical treatment for glaucoma. Research has shown that the number of drainage tube implantations has steadily increased in recent years, while the number of trabeculectomies has correspondingly decreased (Bogunjoko et al., 2019; Arora et al., 2015; Boland et al., 2021).

## 2.2 Statistical analysis

Quantitative data are presented as means ± standard deviation (SD). The changes in IOP, mean deviation (MD) and PSD of VF, RNFL thickness in the macular and peripapillary

regions, VD in the ONH, peripapillary region, and macular area, as well as the area and perimeter of the FAZ at each postoperative follow-up time point were compared to assess dynamic changes following glaucoma surgery. For normally distributed data, paired t-tests were used for comparisons; for non-normally distributed data, the Wilcoxon Signed Ranks Test was employed for analysis.

Univariate and multivariate linear regression analyses were performed to explore potential factors associated with changes in VD. VD in different regions was considered as the dependent variable, while age, gender, IOP, follow-up duration, mean RNFL thickness in the macula, mean RNFL thickness in the optic disc, MD of VF, FAZ area, and FAZ perimeter were included as independent variables in the regression model. All statistical tests were two-sided, with a P-value < 0.05 considered statistically significant. Statistical analyses were performed using SPSS Statistics software, version 27.0.0 (IBM Corporation, New York, NY).

2.3 Surgical technique

The patient is placed in the supine position, and the procedure is performed under local sub-Tenon's anesthesia or general anesthesia. Preoperatively, the eye surrounding skin and conjunctival sac are cleaned with Povidone-Iodine, which is allowed to stay in the conjunctival sac for 2-3 minutes before the surgical field is irrigated with saline. The PGI is typically placed in the temporal-superior quadrant so a Vicryl® traction suture is fixed at the limbal cornea, and the eye is rotated inferonasally, and corneal protection is provided using sodium hyaluronate gel or a moistened sponge. The conjunctiva and Tenon's capsule are incised along the limbus to expose the surgical field. The superficial vessels on the exposed sclera are mechanically removed to achieve initial hemostasis, and minimal electrocoagulation is applied if necessary. Mitomycin C is applied at a concentration of 0.5 mg/mL to the site of the Paul-Tube implantation plate for 2 minutes, followed by thorough irrigation with saline.

The patency of the PGI is confirmed, and the positions of the two rectus muscles are verified. The implantation plate is placed beneath the rectus muscles, approximately 8-10 mm from the limbus, and fixed to the sclera with 9-0 nylon sutures. A 6-0 polypropylene suture is inserted into the drainage tube to prevent excessive early aqueous humor

drainage. The distal end of the drainage tube is trimmed to an appropriate length for smooth insertion into the anterior chamber. A 26G cannula is used to create a scleral tunnel about 2 mm from the limbus, through which the drainage tube is inserted into the anterior chamber. The drainage tube and implantation plate are checked to ensure proper drainage of aqueous humor, and the drainage flow is adjusted by retracting the 6-0 polypropylene suture if necessary. A single or double-layered cover made of Tutoplast® (Tutogen Medical GmbH, 91077 Neunkirchen a.Br., Germany) is cut and placed over the external drainage tube, and the cover is fixed using fibrin glue. The 6-0 suture within the drainage tube is typically placed in an infero-temporal sub-conjunctival pocket. The conjunctival incisions are sutured with 10-0 nylon sutures. At the end of the procedure, gentamicin and dexamethasone are injected into the inferior subconjunctival space. Postoperatively, the patient is prescribed dexamethasone eye drops (six times daily), ofloxacin eye drops (four times daily), and atropine eye drops (once daily). The polypropylene suture within the drainage tube can be removed during a postoperative slit-lamp examination at the outpatient clinic.

2.4 Examination Procedures and Criteria

All study participants underwent comprehensive ophthalmic evaluations and medical history collection, including a detailed history of systemic conditions, prior anti-glaucoma surgeries, current glaucoma eye drop medications, BCVA, IOP measured using the GAT, and baseline cup-to-disc ratio (CDR) and other baseline parameters.

At preoperative and postoperative follow-up visits at 1 week, 1 month, 3 months, and 6 months, in addition to routine ophthalmic examinations, all patients underwent OCT and OCTA scans of the macular and optic disc regions. These examinations were performed using the Heidelberg HRA+OCT Spectralis system, and RNFL thickness parameters were collected for both the macular and peripapillary regions.

The macular OCT images were divided using the Early Treatment Diabetic Retinopathy Study (ETDRS) grid, centered on the fovea, and subdivided into nine subfields: a central 1-mm circle, an inner ring (1–3 mm), and an outer ring (3–6 mm), with the inner and outer rings further divided into superior, inferior, nasal, and temporal quadrants. The average RNFL thickness for each region was calculated by averaging the corresponding values

from the outer and inner rings. For example, the RNFL thickness of the superior region was obtained by averaging the values from the superior outer and superior inner region (Figure 1a).

The OCT images of the ONH and peripapillary region were automatically segmented by the machine into nasal, NS, TS, temporal, TI, NI and the average value of the entire peripapillary region(G). The NS and TS regions were combined into the superior region, and the TI and NI regions were combined into the Inferior region for analysis（Figure 1b).

Furthermore, at the preoperative and 6-month postoperative follow-up visits, all patients underwent visual field testing using the Humphrey Field Analyzer with the 24-2 program.

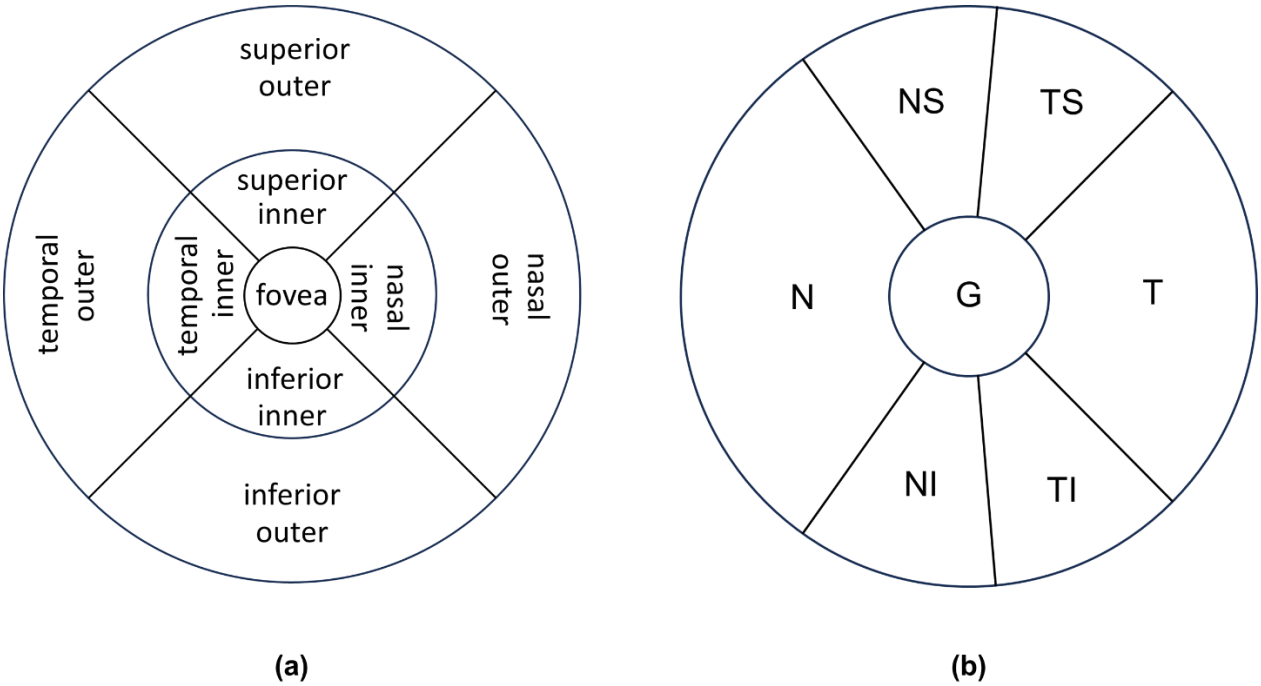


**Figure 1:** Segmentation of the macular and peripapillary regions in OCT images. (a) Macular region (b) Peripapillary region.

### 2.4.1 OCTA examination

All OCTA images were acquired using the Zeiss Plex Elite 9000 system. OCT and OCTA scans were performed at the preoperative and each postoperative follow-up visit, with images having a signal strength $\leqslant$ 6 being excluded. The macular scan areas were

selected as 3 mm × 3 mm and 6 mm × 6 mm (centered on the fovea), while the optic disc and peripapillary region scan area was 6 mm × 6 mm, centered on the ONH. The macular area was segmented into superficial (upper limit = Inner Limiting Membrane, lower limit = Inner Plexiform Layer-10 μm) and deep (upper limit = Inner Plexiform Layer-10μm, lower limit = Outer Plexiform Layer) layer, and full-thickness retinal vascular imaging was also collected, with full-thickness retina defined as the combination of the superficial and deep layers. All scans were performed without pharmacological pupil dilation.

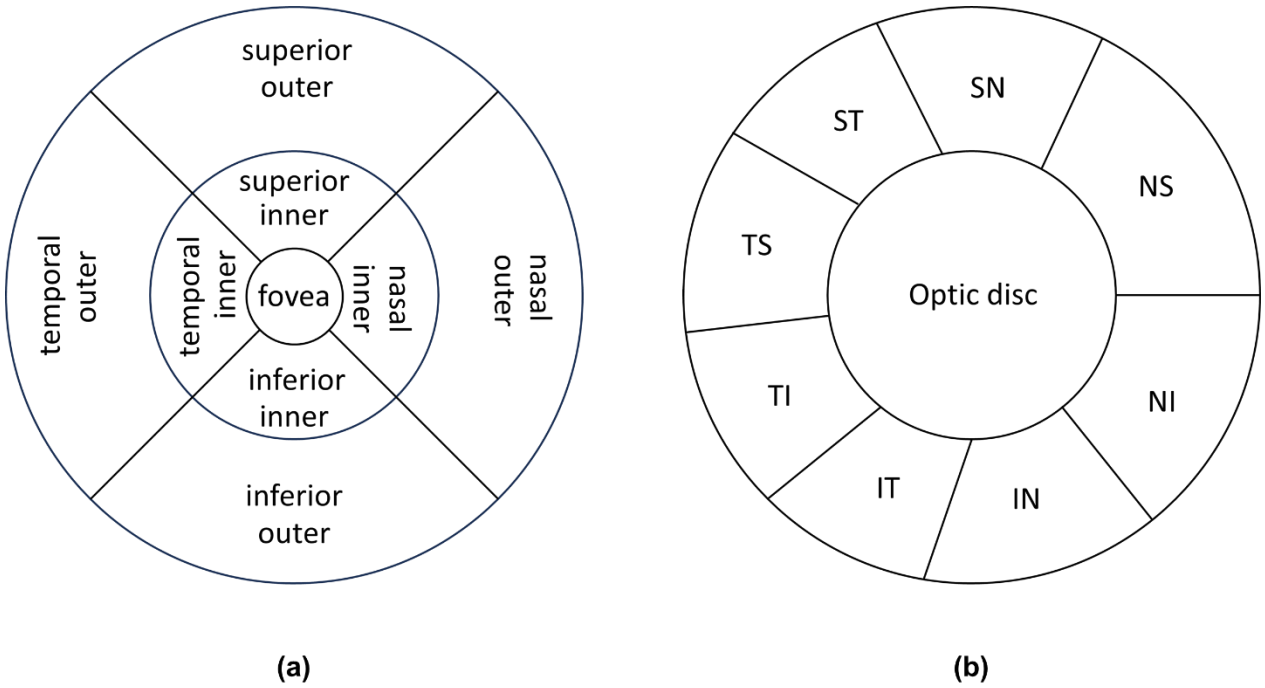


**Figure 2:** Segmentation of the macular and peripapillary regions in OCTA images. (a) Macular region (b) Peripapillary region.

VD data extraction process: Scanning images were extracted from the OCTA device and imported into ImageJ software (http://rsb.info.nih.gov/ij/index.html, provided by the National Institutes of Health, Bethesda, Maryland, USA). The radial peripapillary capillaries (RPC) in the peripapillary region were divided into eight sectors based on the Garway-Heath map, including the superior temporal (ST) , superior nasal (SN) , inferior temporal (IT) , inferior nasal (IN) , superior nasal (SN) , inferior nasal (IN) , inferior temporal

(IT) , and superior temporal (ST) quadrants (Garway-Heath et al., 2000)(Figure 2b). The macular area was divided using the Early Treatment Diabetic Retinopathy Study (ETDRS) grid, centered on the fovea, and subdivided into nine subfields: a central 1mm circle, an inner ring (1–3 mm), and an outer ring (3–6 mm), with each of the inner and outer rings further divided into superior, inferior, nasal, and temporal quadrants(Figure 2a).

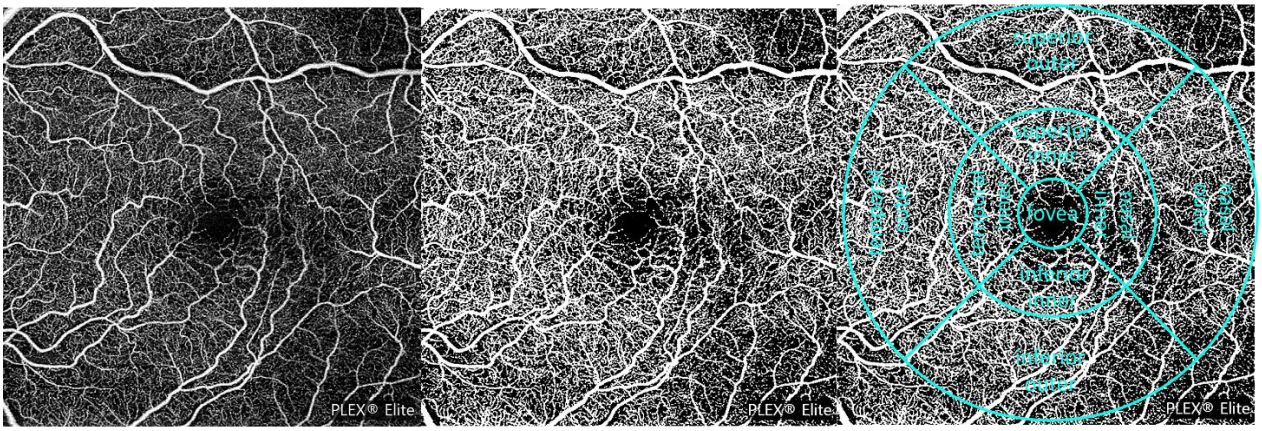


**(a)** **(b)** **(c)**

**Figure 3:** Processing of OCTA images in ImageJ (using 6 mm × 6 mm macular region as an example). (a) Original image in OCTA (b) Binarized image in ImageJ (c) Segmentation of the 6 mm × 6 mm macular region.

In ImageJ, the images were binarized, with white pixels representing vessels and black pixels representing the background (Figure 3b). VD was defined as the percentage of vascular pixels relative to the total area. Additionally, FAZ was measured using the 6×6 mm full-thickness macular retinal image. The FAZ contour was manually delineated, and the pixel area and perimeter were automatically calculated by ImageJ software.

# 3 Results

## 3.1 Baseline Characteristics of the Patients

A total of 20 eyes from 20 glaucoma patients who underwent PGI surgery met the inclusion criteria and underwent serial OCTA imaging(

Table **1**). The baseline characteristics of the patients are summarized in Table 1. The mean age of the cohort was 63.20 ± 13.38 years, with six patients (30 %) being female. Fifteen patients (75 %) had a prior history of glaucoma surgery. The mean number of anti-glaucoma medications decreased significantly from 3.16 ± 1.70 preoperatively to 0.70 ± 1.06 at six months postoperatively ($p < 0.001$).

BCVA remained stable, with preoperative and six-month postoperative values of 0.48 ± 0.31 and 0.47 ± 0.26, respectively ($p = 0.798$).

**Table 1:** Characteristics of 20 Glaucoma Patients.

| Variables | | | means±SD | | p Value |
|---|---|---|---|---|---|
| **Age, year** | | | 63.20 ± 13.38 | | |
| **Female** | | | 6(30%) | | |
| **Previous glaucoma surgery** | | | 15(75%) | | |
| **No.of medications** | | | | | |
| Baseline | | | 3.16 ± 1.70 | | |
| Postoperative 6 month | | | 0.70 ± 1.06 | | **<0.001** |
| **Visual field MD, dB** | | | | | |
| Baseline | | | -12.49 ± 14.30 | | |
| Postoperative 6 month | | | -15.83 ± 10.59 | | 0.353 |
| **Visual field Visual Field Index (VFI)** | | | | | |
| Baseline | | | 0.667±0.297 | | |
| Postoperative 6 month | | | 0.599±0.310 | | 0.172 |
| **Visual field PSD, dB** | | | | | |
| Baseline | | | 7.944± 3.617 | | |
| Postoperative 6 month | | | 8.03± 3.917 | | 0.08 |
| **BCVA** | | | | | |
| Baseline | | | 0.48 ± 0.31 | | |
| Postoperative 6 month | | | 0.47 ± 0.26 | | 0.798 |
| **IOP, mmHg** | | | | | |
| Baseline | | | 22.26 ± 7.66 | | |
| Postoperative 1 week | | | 18.5 ± 9.56 | | 0.058 |
| Postoperative 1 month | | | 15.46 ± 5.29 | | **0.029** |
| Postoperative 3 month | | | 13.86 ± 7.29 | | **0.034** |
| Postoperative 6 month | | | 12.01 ± 2.10 | | **0.005** |
| **mRNFL thickness, lm** | | | | | |
| Baseline | | | 304.19 ± 41.47 | | |
| Postoperative 1 week | | | 322.92 ± 58.73 | | **0.007** |
| Postoperative 1 month | | | 298.72 ± 29.80 | | **0.046** |
| Postoperative 3 month | | | 292.34 ± 28.19 | | 0.107 |
| Postoperative 6 month | | | 305.61 ± 40.22 | | **0.004** |
| **pRNFL thickness, lm** | | | | | |
| Baseline | | | 63.48 ± 26.49 | | |
| Postoperative 1 week | | | 72.81 ± 31.49 | | 0.189 |
| Postoperative 1 month | | | 58.77 ± 25.45 | | 0.193 |
| Postoperative 3 month | | | 66.21 ± 23.96 | | 0.905 |
| Postoperative 6 month | | | 70.70 ± 36.99 | | **0.004** |
| **FAZ prei., mm** | | | | | |
| Baseline | | | 2.66 ± 0.49 | | |
| Postoperative 1 week | | | 2.51 ± 0.48 | | 0.615 |
| Postoperative 1 month | | | 2.54 ± 0.45 | | 0.577 |
| Postoperative 3 month | | | 2.34 ± 0.43 | | **0.003** |
| Postoperative 6 month | | | 2.45 ± 0.41 | | **0.024** |
| **FAZ area, mm²** | | | | | |
| Baseline | | | 0.38 ± 0.13 | | |
| Postoperative 1 week | | | 0.35 ± 0.12 | | 0.606 |
| Postoperative 1 month | | | 0.36 ± 0.14 | | 0.287 |
| Postoperative 3 month | | | 0.31 ± 0.14 | | **0.016** |
| Postoperative 6 month | | | 0.34 ± 0.12 | | **0.023** |

## 3.2 OCTA Data Analysis

These results demonstrate the changes in retinal microvascular flow density in glaucoma patients within six months following PGI surgery, with varying impacts observed across different regions.

### 3.2.1 OCTA 3 mm × 3 mm Macular Region

#### 3.2.1.1 Superficial Retinal Layer

OCTA 3 mm × 3 mm Macular VD Changes in the Superficial Retinal Layer

Using the ETDRS grid, the macular VD was analyzed in the fovea, inferior, superior, nasal and temporal regions. Significant changes were observed in the Fovea, Nasal, and Temporal regions in the superficial layer.

In the fovea, superficial retinal VD increased from 0.172±0.060 preoperatively to a peak of 0.229±0.072 at three months, though this change was not statistically significant ($p = 0.065$). However, significant increases were noted at one week (0.203±0.067, $p = 0.027$) and one month (0.208±0.058, $p = 0.045$). By six months, VD slightly decreased to 0.202±0.032 ($p = 0.064$) but remained above baseline (Figure 4a).

In the inferior region, VD reached a maximum of 0.370±0.068 at three months ($p = 0.376$), though without statistical significance. No significant changes were observed at one week (0.328±0.071, $p = 0.857$) or one month (0.355±0.068, $p = 0.425$). At six months, VD declined to 0.314±0.090 ($p = 0.459$) (Figure 4b).

In the nasal region, VD increased from 0.320±0.075 preoperatively to 0.365±0.062 at three months ($p = 0.017$). Significant increases were detected at one week (0.362±0.071, $p = 0.019$) and one month (0.359±0.063, $p = 0.029$), while at six months, VD declined to 0.341±0.059 ($p = 0.186$) but remained above baseline (Figure 4c).

In the superior region, VD showed no statistically significant variation throughout follow-up, with values increasing from 0.352±0.100 preoperatively to 0.372±0.064 at six months ($p = 0.880$). The changes at one week (0.366±0.083, $p = 0.500$), one month (0.363±0.059, $p = 0.642$), and three months (0.365±0.059, $p = 0.797$) were also not significant (Figure 4d).

In the temporal region, VD peaked at 0.333±0.047 at three months (p = 0.060). Statistically significant increases were observed at one week (0.323±0.067, p = 0.013) and one month (0.327±0.327, p = 0.011). By six months, VD slightly decreased to 0.314±0.030 (p = 0.102) but remained higher than baseline (Figure 4e).

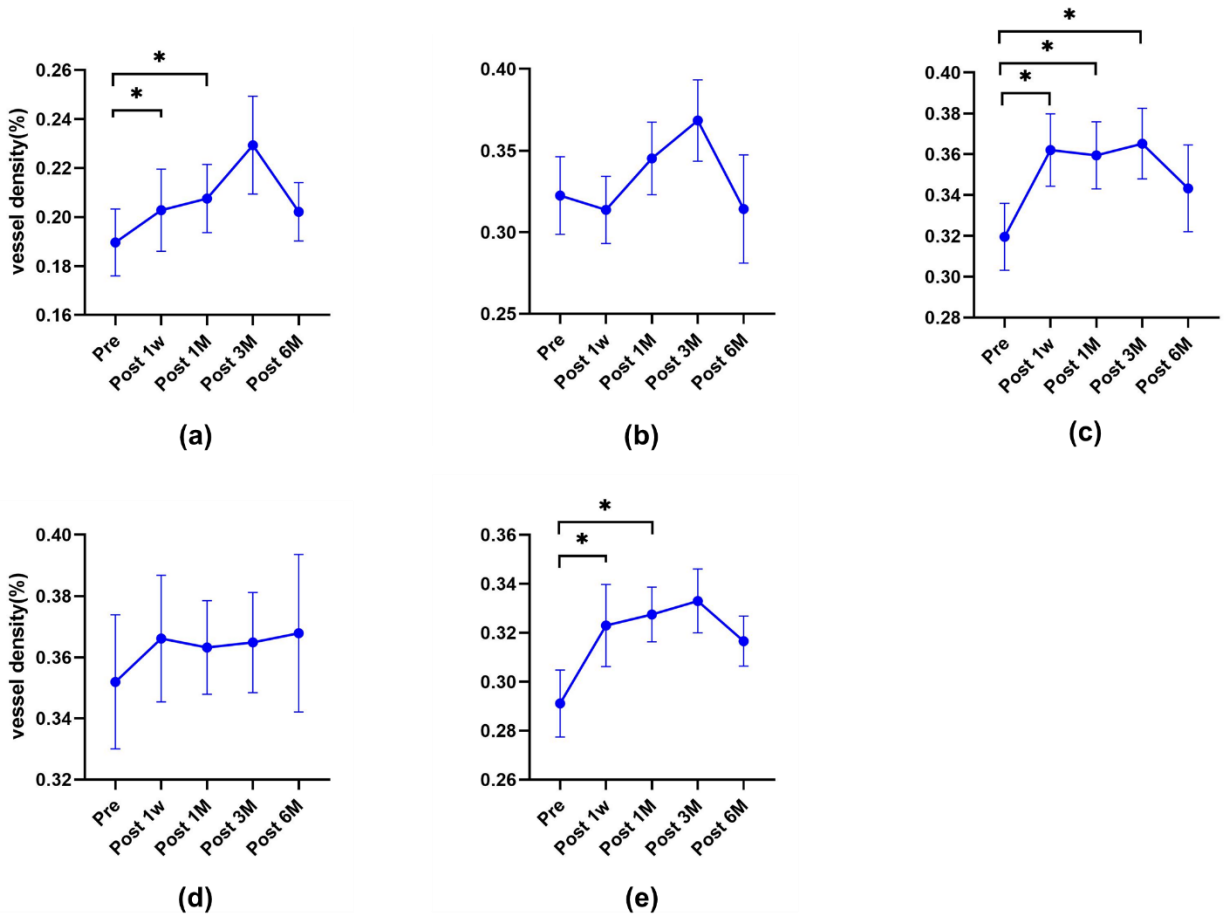


**Figure 4:** Superficial Retinal Layer vascular density in the fovea and each subregion of the inner ring within the 3 mm × 3 mm macular area. (a) Fovea region (b) Inferior-inner region (c) Nasal-inner region (d) Superior-inner region (e) Temporal-inner region

3.2.1.2 Deep Retinal Layer

OCTA 3 mm × 3 mm Macular VD Changes in the Deep Retinal Layer

Significant changes in VD were observed in the fovea, inferior, superior, and temporal regions.

In the fovea, deep retinal VD increased from a preoperative value of 0.210±0.094 to a peak of 0.245±0.128 at three months, demonstrating statistical significance (p = 0.022). A transient decrease was noted at one week (0.159±0.060, p = 0.583), followed by a significant rise at one month (0.202±0.092, p = 0.010). By six months, VD slightly declined to 0.220±0.061 (p = 0.063) but remained higher than baseline (Figure 5a).

In the inferior region, VD initially decreased at one week (0.391±0.069 vs. 0.404±0.077 preoperatively, p = 0.836). However, a progressive increase was observed at one month (0.434±0.088, p = 0.047), three months (0.445±0.043, p = 0.133), and six months (0.451±0.071, p = 0.091), though this trend did not reach statistical significance(Figure 5b).

In the nasal region, VD declined from baseline (0.406±0.082) to 0.388±0.063 at one week (p = 0.959), then increased at one month (0.427±0.079, p = 0.069) and three months (0.449±0.062, p = 0.087). At six months, VD slightly decreased to 0.416±0.060 (p = 0.735) but remained above baseline. None of these changes were statistically significant (Figure 5c).

In the superior region, VD reached its peak at one month (0.450±0.060, p = 0.005), showing a significant increase from baseline (0.412±0.084). Although VD rose slightly at one week (0.414±0.067, p = 0.469), the trend plateaued at three months (0.444±0.044, p = 0.249), followed by a minor decline at six months (0.445±0.055, p = 0.091) (Figure 5d).

In the temporal region, a pattern similar to the superior region was observed. VD increased from a preoperative value of 0.378±0.073 to a peak of 0.423±0.054 at one month (p = 0.002). No significant changes were noted at one week (0.382±0.067, p = 0.679) or three months (0.409±0.043, p = 0.311). By six months, VD elevated to 0.419±0.032 (p = 0.018), showing a statistically significant increase from baseline (Figure 5e).

Overall, VD at six months remained higher than preoperative levels across all deep retinal regions, but only the temporal region showed a statistically significant increase over time.

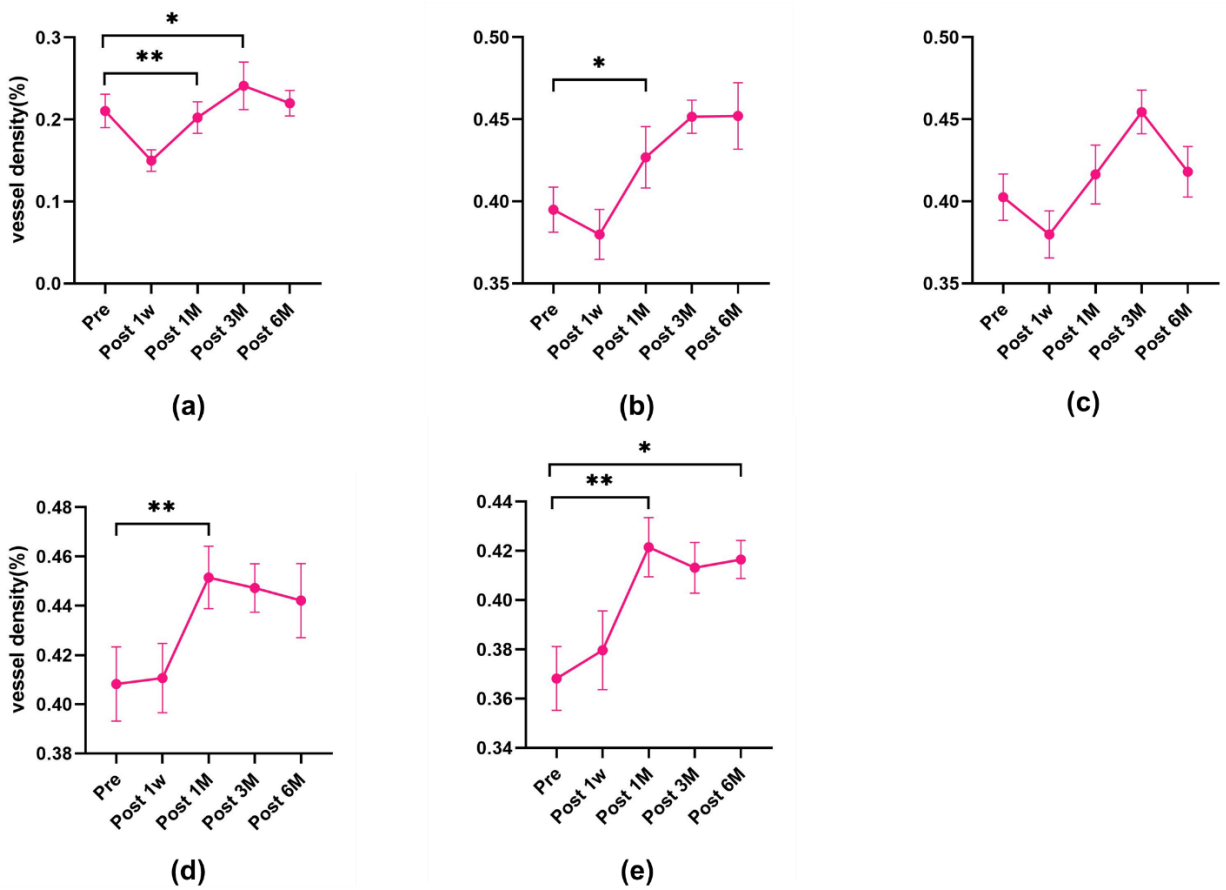


**Figure 5:** Deep Retinal Layer vascular density in the fovea and each subregion of the inner ring within the 3 mm × 3 mm macular area. (a) Fovea region (b) Inferior-inner region (c) Nasal-inner region (d) Superior-inner region (e) Temporal-inner region.

3.2.1.3 Full-Thickness Retina

OCTA 3 mm × 3 mm Macular VD Changes in the Full-Thickness Retina

Significant changes in VD were observed in the fovea, inferior, and temporal regions.

In the fovea, VD increased from 0.227±0.086 preoperatively to a peak of 0.266±0.099 at three months, demonstrating statistical significance ($p = 0.033$). A transient decrease was noted at one week (0.214±0.071, $p = 0.109$), followed by a significant rise at one month (0.247±0.083, $p = 0.015$). By six months, VD declined slightly to 0.237±0.058 ($p = 0.063$) but remained higher than baseline (Figure 6a).

In the inferior region, VD showed a minor decrease at one week (0.381±0.059 vs. 0.392±0.072 preoperatively, p = 0.605), followed by a progressive increase at one month (0.423±0.071), three months (0.430±0.042), and a peak at six months (0.433±0.057). Among these, only the increase at one month was statistically significant compared to baseline (p = 0.031) (Figure 6b).

In the nasal region, VD declined slightly at one week (0.403±0.054, p = 0.379) from its baseline of 0.407±0.078, followed by an increase at one month (0.427±0.060, p = 0.156) and a peak at three months (0.446±0.053, p = 0.133). By six months, VD returned to near-baseline levels (0.411±0.051, p = 1.000). However, none of these changes reached statistical significance (Figure 6c).

In the superior region, VD gradually increased from 0.400±0.081 at baseline to 0.442±0.041 at six months, but this trend was not statistically significant (p = 0.128). None of the time points showed significant differences from baseline (Figure 6d).

In the temporal region, VD increased from 0.367±0.068 preoperatively to a peak of 0.413±0.018 at six months, a statistically significant change (p = 0.018). A moderate increase was observed at one week (0.381±0.059, p = 0.134), followed by a further rise at one month (0.409±0.048, p = 0.009), with the latter showing statistical significance (Figure 6e）.

Overall, VD at six months remained higher than baseline across all full-thickness retinal regions. However, only the temporal region showed a statistically significant increase over time.

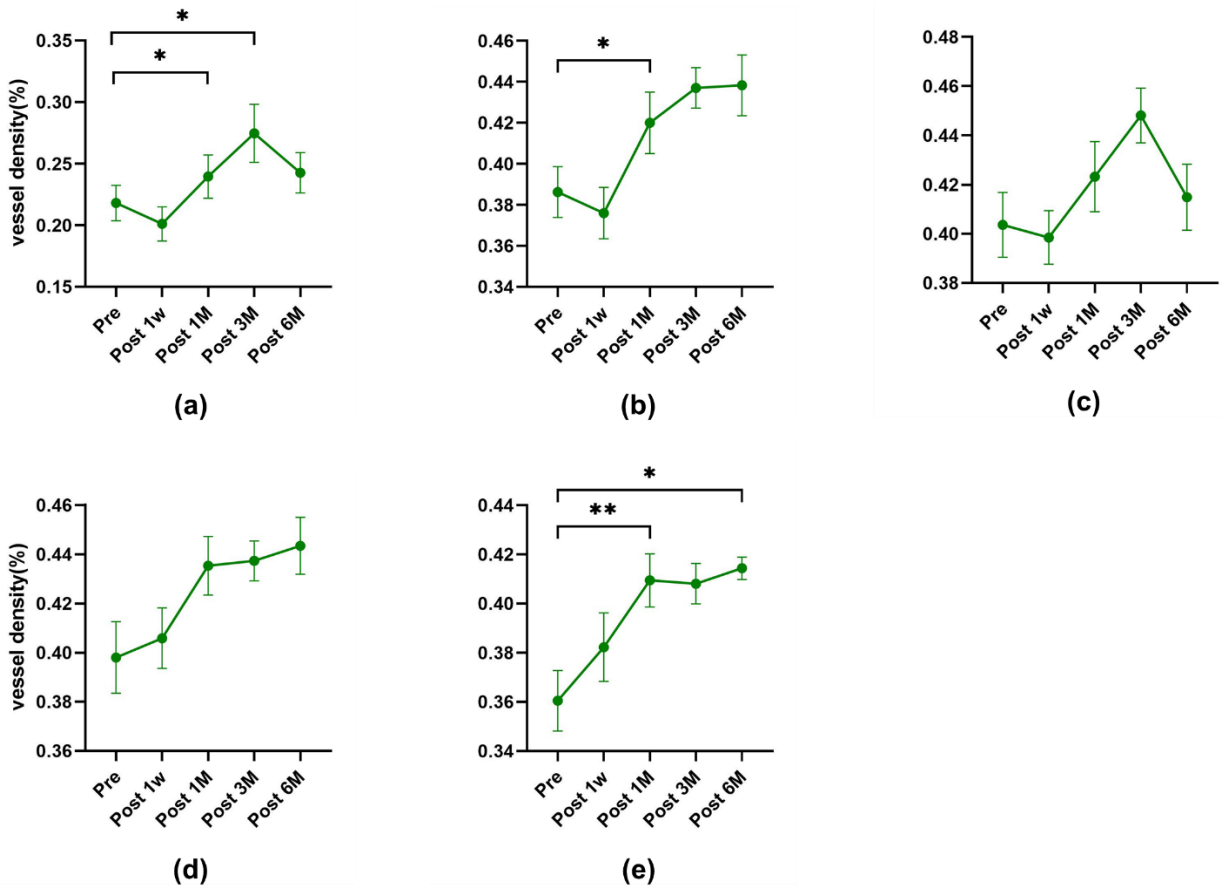


**Figure 6:** Full-thickness Retina vascular density in the fovea and each subregion of the inner ring within the 3 mm × 3 mm macular area. (a) Fovea region (b) Inferior-inner region (c) Nasal-inner region (d) Superior-inner region (e) Temporal-inner region

### 3.2.2 OCTA 6 mm × 6 mm Macular Region

The OCTA 6 mm × 6 mm macular images were analyzed based on the ETDRS grid, dividing the macular region into the Fovea, Parafoveal, and Perifoveal zones. As the Fovea and Parafoveal regions have already been comprehensively analyzed in the 3 mm × 3 mm macular images, these areas will not be further discussed in the 6 mm × 6 mm analysis. The perifoveal zone is further subdivided into inferior, nasal, superior, and temporal subregions.

In the 6 mm × 6 mm macular images, except for the temporal subregion in the superficial retinal layer, all subregions showed an increase in VD at six months postoperatively

compared to baseline. However, none of these changes reached statistical significance(Figure 7,Figure 8,Figure 9).

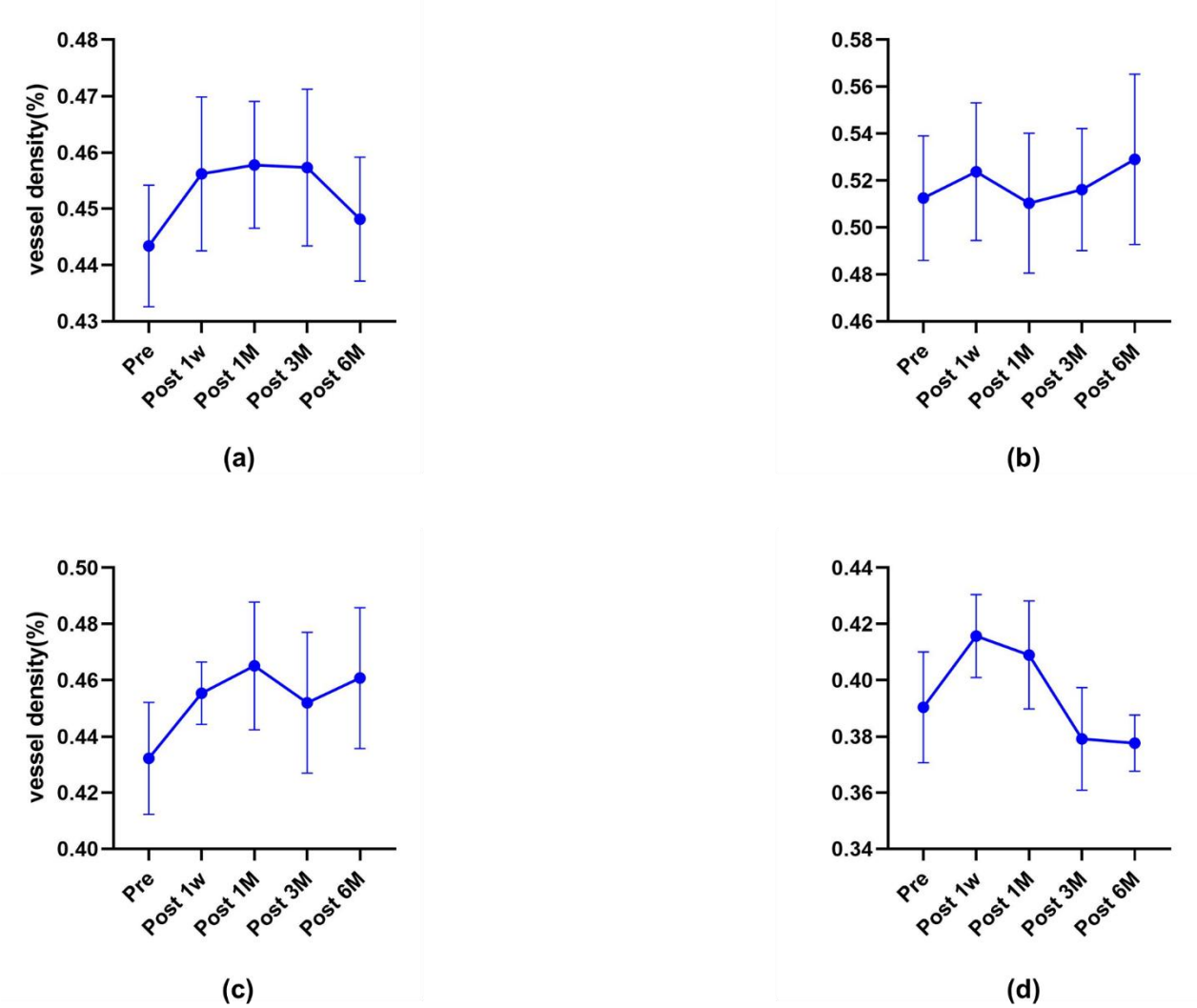


**Figure 7:** Superficial retinal vascular density in each subregion of the outer ring within the 6 mm × 6 mm macular area. (a) Inferior-outer region (b) Nasal-outer region (c) Superior-outer region (d) Temporal-outer region.

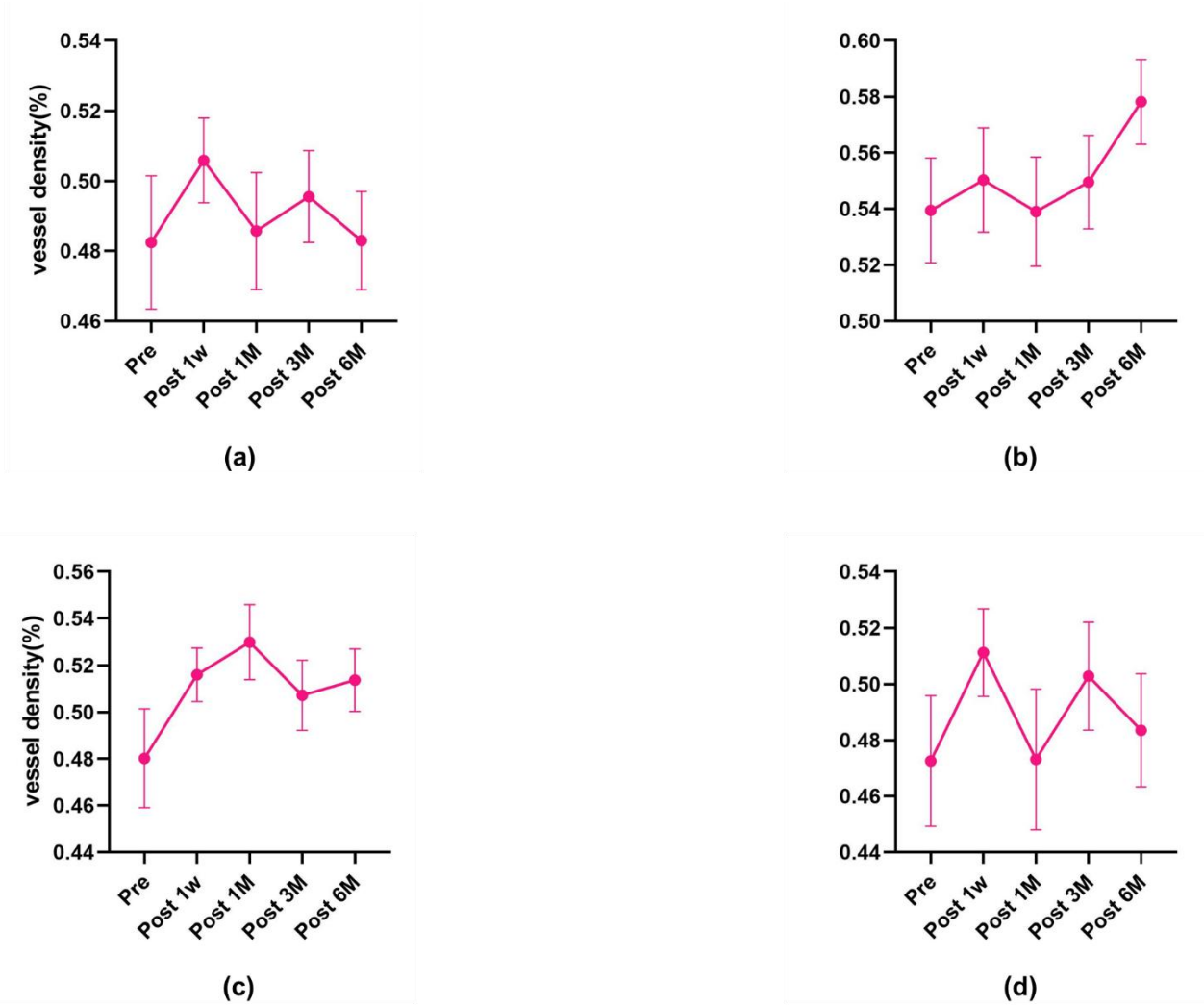


**Figure 8:** Deep retinal vascular density in each subregion of the outer ring within the 6 mm × 6 mm macular area. (a) Inferior-outer region (b) Nasal-outer region (c) Superior-outer region (d) Temporal-outer region.

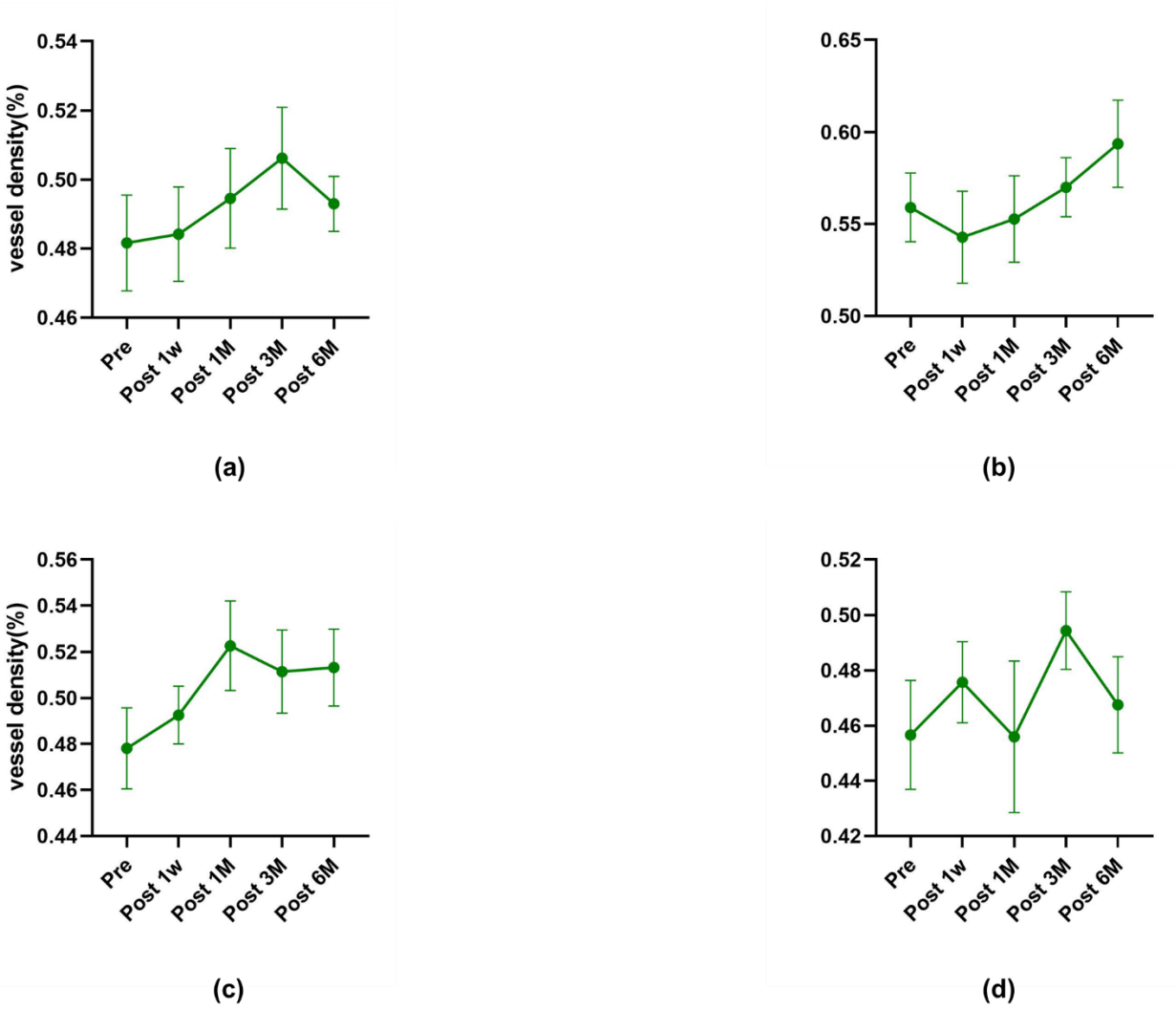


**Figure 9:** Full-thickness retina vascular density in each subregion of the outer ring within the 6 mm × 6 mm macular area. (a) Inferior-outer region (b) Nasal-outer region (c) Superior-outer region (d) Temporal-outer region.

### 3.2.3 ONH and Peripapillary Region

The OCTA 6 mm × 6 mm ONH and peripapillary region images were analyzed using the Garway-Heath classification, dividing the region into the central ONH zone and eight peripapillary subregions.

Among the three retinal layers and nine subregions, a decrease in VD at six months postoperatively compared to baseline was observed in the NI and ST subregions of the superficial retinal layer, the ST subregion of the deep retinal layer, and the ST subregion

of the full retinal layer. In all other subregions across different retinal layers, VD at six months postoperatively was higher than baseline.

In the deep retinal layer, the ONH region showed a significant increase in VD at one week (0.529 ± 0.116, p = 0.040) and six months (0.563 ± 0.058, p = 0.039) postoperatively. No other subregions or retinal layers demonstrated statistically significant changes(Figure 10,Figure 11,Figure 12).

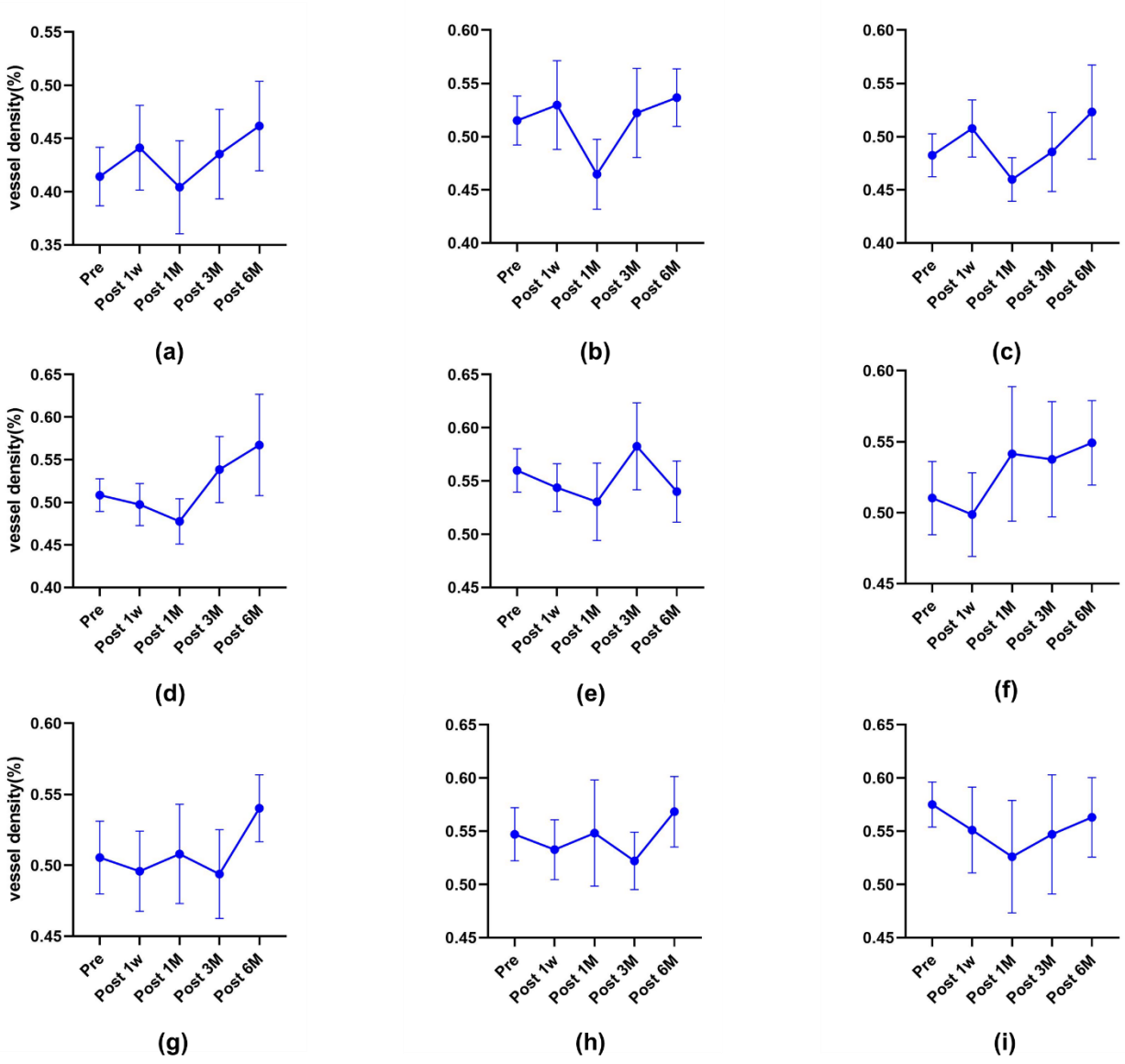


**Figure 10:** Superficial retinal vascular density in the peripapillary area, including the optic disc and each subregion. (a) Optic disc (b) SN region (c) NS region (d) NI region (e) IN region (f) IT region (g) TI region (h) TS region (i) ST region.

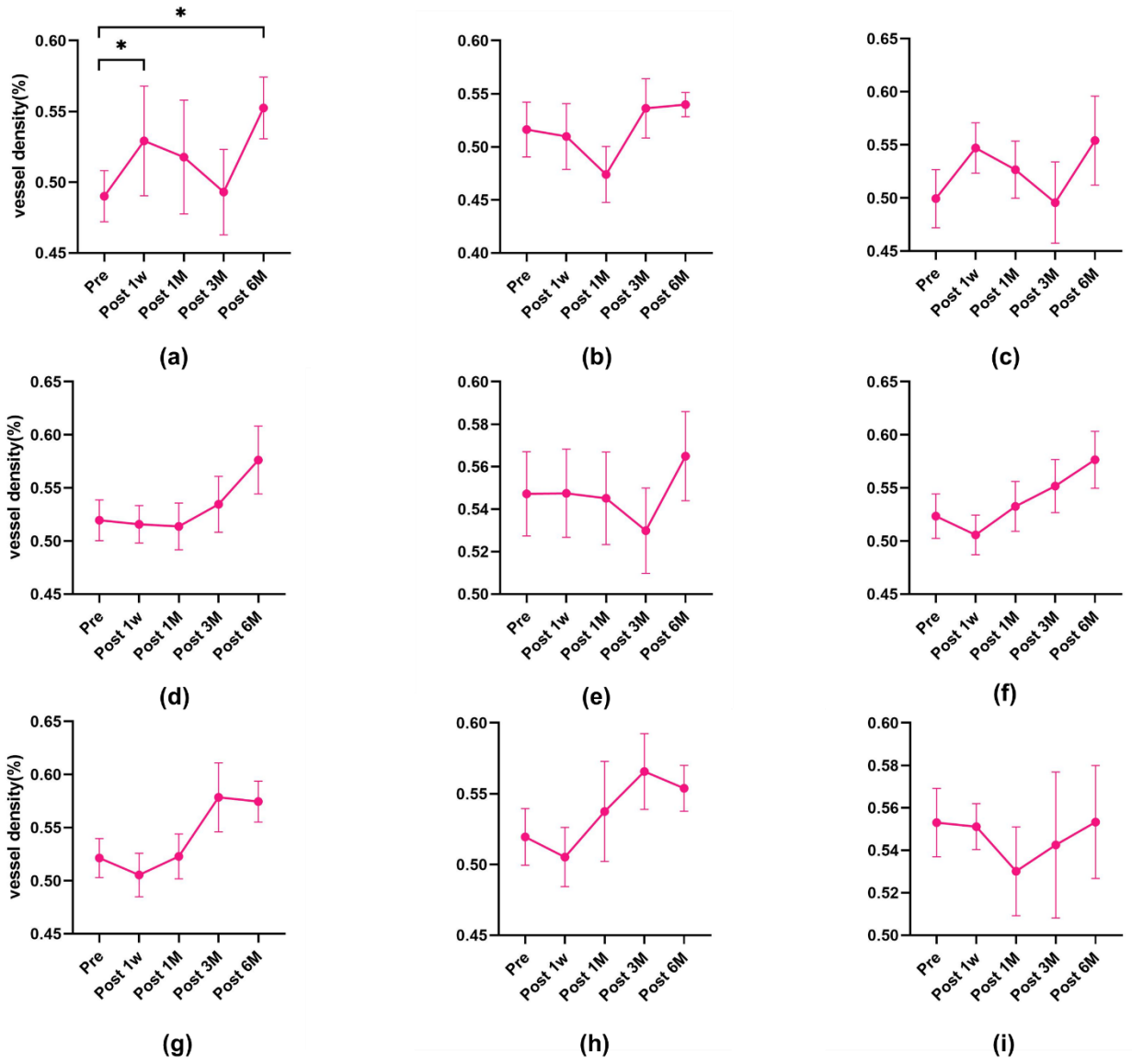


**Figure 11:** Deep retinal vascular density in the peripapillary area, including the optic disc and each subregion. (a) Optic disc (b) SN region (c) NS region (d) NI region (e) IN region (f) IT region (g) TI region (h) TS region (i) ST region.

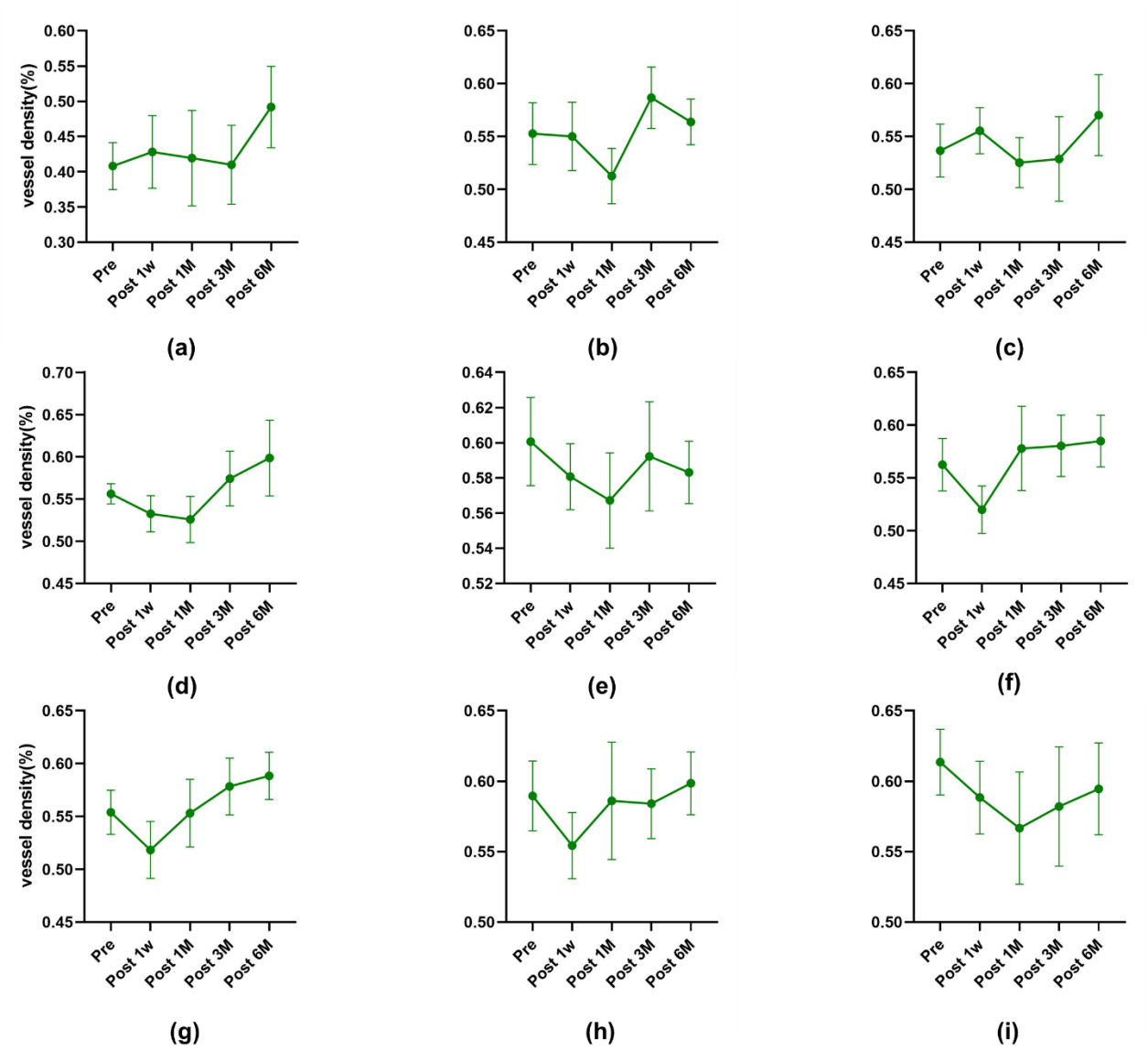


**Figure 12:** Full-thickness retina vascular density in the peripapillary area, including the optic disc and each subregion. (a) Optic disc (b) SN region (c) NS region (d) NI region (e) IN region (f) IT region (g) TI region (h) TS region (i) ST region

### 3.2.4 FAZ Area and Perimeter

In the OCTA 6 mm × 6 mm macular full-thickness retinal images, the FAZ perimeter and area were manually traced.

Both FAZ perimeter and area showed a progressive reduction throughout the follow-up period. The FAZ perimeter reached its minimum value at three months postoperatively (2.343 ± 0.434, $p = 0.003$) before showing a slight increase at six months postoperatively

(2.452 ± 0.413, p = 0.024); however, it remained lower than the baseline value, with both time points demonstrating statistically significant changes. Similarly, the FAZ area decreased to its lowest value at three months postoperatively (0.31 ± 0.14, p = 0.016), followed by a modest increase at six months postoperatively (0.34 ± 0.12, p = 0.023), yet still remained reduced compared to baseline. Both of these time points showed statistically significant changes (Figure 13).

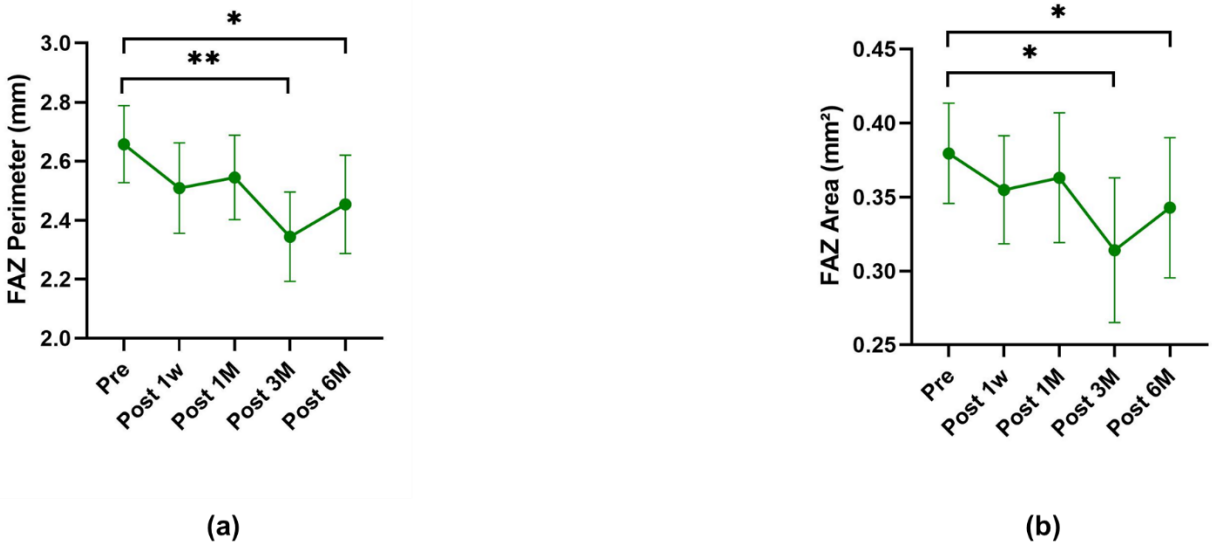


**Figure 13:** Changes in FAZ perimeter and area over time. (a) FAZ perimeter (b) FAZ area

In the OCTA 6 mm × 6 mm macular full-thickness retinal images, the FAZ perimeter and area were manually traced.

Both FAZ perimeter and area showed a progressive reduction throughout the follow-up period. The FAZ perimeter reached its minimum value at three months postoperatively (2.343 ± 0.434, p = 0.003) before showing a slight increase at six months postoperatively (2.452 ± 0.413, p = 0.024); however, it remained lower than the baseline value, with both time points demonstrating statistically significant changes. Similarly, the FAZ area decreased to its lowest value at three months postoperatively (0.31 ± 0.14, p = 0.016), followed by a modest increase at six months postoperatively (0.34 ± 0.12, p = 0.023), yet still remained reduced compared to baseline. Both of these time points showed statistically significant changes.

## 3.3 OCT RNFL Analysis

The OCT images of the macula and ONH and peripapillary regions revealed a significant increase in RNFL thickness one-week post-surgery, followed by a gradual decline. By the six-month postoperative follow-up, the RNFL thickness had nearly returned to the preoperative baseline level.

### 3.3.1 Macular Region

The OCT macular images were divided into the fovea, inferior, nasal, superior, and temporal regions using the ETDRS chart. In each region, the RNFL thickness increased to its peak one-week post-surgery, but a sharp decline in RNFL thickness was observed at one-month post-surgery. Except for the nasal region, RNFL thickness dropped below the preoperative baseline in all other regions. After one month, RNFL values in most regions, except for the superior region, showed a subsequent rise. However, by the six-month postoperative follow-up, RNFL thickness showed varying trends across regions. In the fovea region, RNFL thickness at six months (292.231±35.637) was lower than preoperative values (301.250±58.874). In the inferior region, RNFL thickness at six months (298.538±26.980) was higher than preoperative values (294.875±35.610). In the nasal region, RNFL thickness at six months (314.500±34.720) was lower than preoperative values (315.950±37.539). In the superior region, RNFL thickness at six months (287.346±44.993) was lower than preoperative values (304.650±33.0196). In the temporal region, RNFL thickness at six months (292.50±23.581) was higher than preoperative values (291.80±33.698). None of these changes were statistically significant.

When comparing the overall mean RNFL thickness in the OCT macular region, it followed the pattern observed in the individual regions. RNFL thickness increased from a preoperative value of 301.705±40.967 to 317.531±56.104 one-week post-surgery, a change that was statistically significant ($p = 0.007$). At one-month post-surgery, RNFL thickness decreased sharply to 295.785±29.613 ($p = 0.046$). At three months post-surgery, RNFL thickness further decreased to 290.357±26.864 ($p = 0.107$), but by six months post-surgery, RNFL thickness showed a trend of recovery (297.023±34.276, $p = 0.004$). This change was statistically significant, though the thickness remained lower than the preoperative baseline (Figure 14).

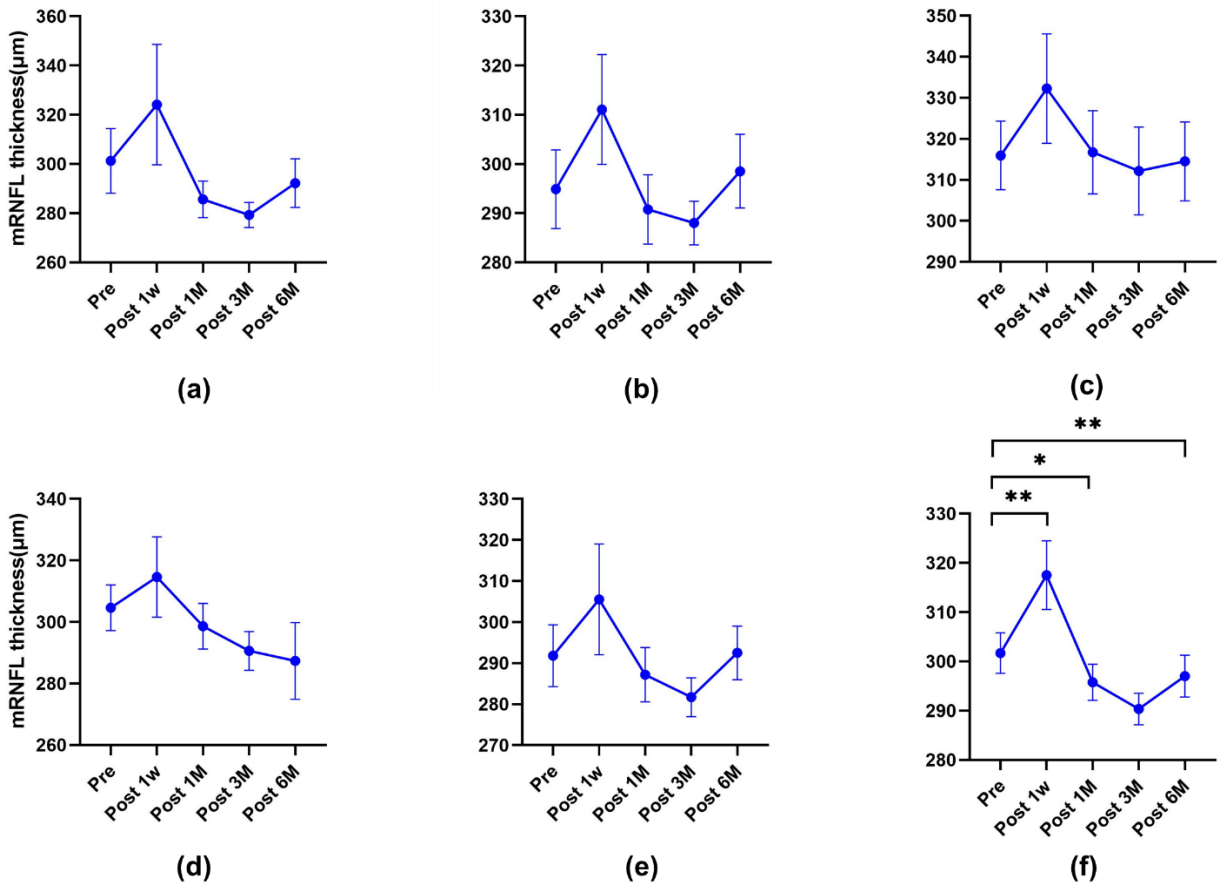


**Figure 14:** Average RNFL thickness in the macular fovea and its subregions. (a) Fovea (b) Inferior region (c) Nasal region (d) Superior region (e) Temporal region (f) Average RNFL thickness across the entire macular area.

3.3.2 Peripapillary Region

The OCT images of the ONH and peripapillary region were automatically segmented by the machine into nasal, NS, TS, temporal, TI, NI and the average value of the entire peripapillary region(G). The NS and TS regions were combined into the superior region, and the TI and NI regions were combined into the Inferior region for analysis.

Except for the nasal region, RNFL thickness in the other regions reached its peak at one week post-surgery, followed by either an increase or decrease. By the six-month postoperative follow-up, RNFL thickness showed varying trends across regions. In the Inferior region, RNFL thickness at six months (66.346±26.724) was lower than preoperative values (68.90±25.687). In the nasal region, RNFL thickness at six months (61.769±50.050) was higher than preoperative values (51.30±25.209). In the superior region, RNFL thickness at six months (63.615±25.20) was lower than preoperative values

(69.750±31.290). In the temporal region, RNFL thickness at six months (66.0±29.397) was higher than preoperative values (62.350±27.124). Among these comparisons, only the change in the Inferior region (p = 0.021) was statistically significant; all other changes were not statistically significant.

When comparing the overall mean RNFL thickness in the OCT peripapillary region(G), the changes followed the trends observed in the individual regions. RNFL thickness increased from a preoperative value of 62.50±23.25 to 66.923±27.75 one-week post-surgery (p = 0.742). At one-month post-surgery, RNFL thickness decreased to 65.667±27.730 (p = 0.793). At three months post-surgery, RNFL thickness further decreased to 63.286±21.567 (p = 0.462). However, by six months post-surgery, RNFL thickness showed a trend of recovery (64.154±27.027, p = 0.596). The change was not statistically significant (Figure 15).

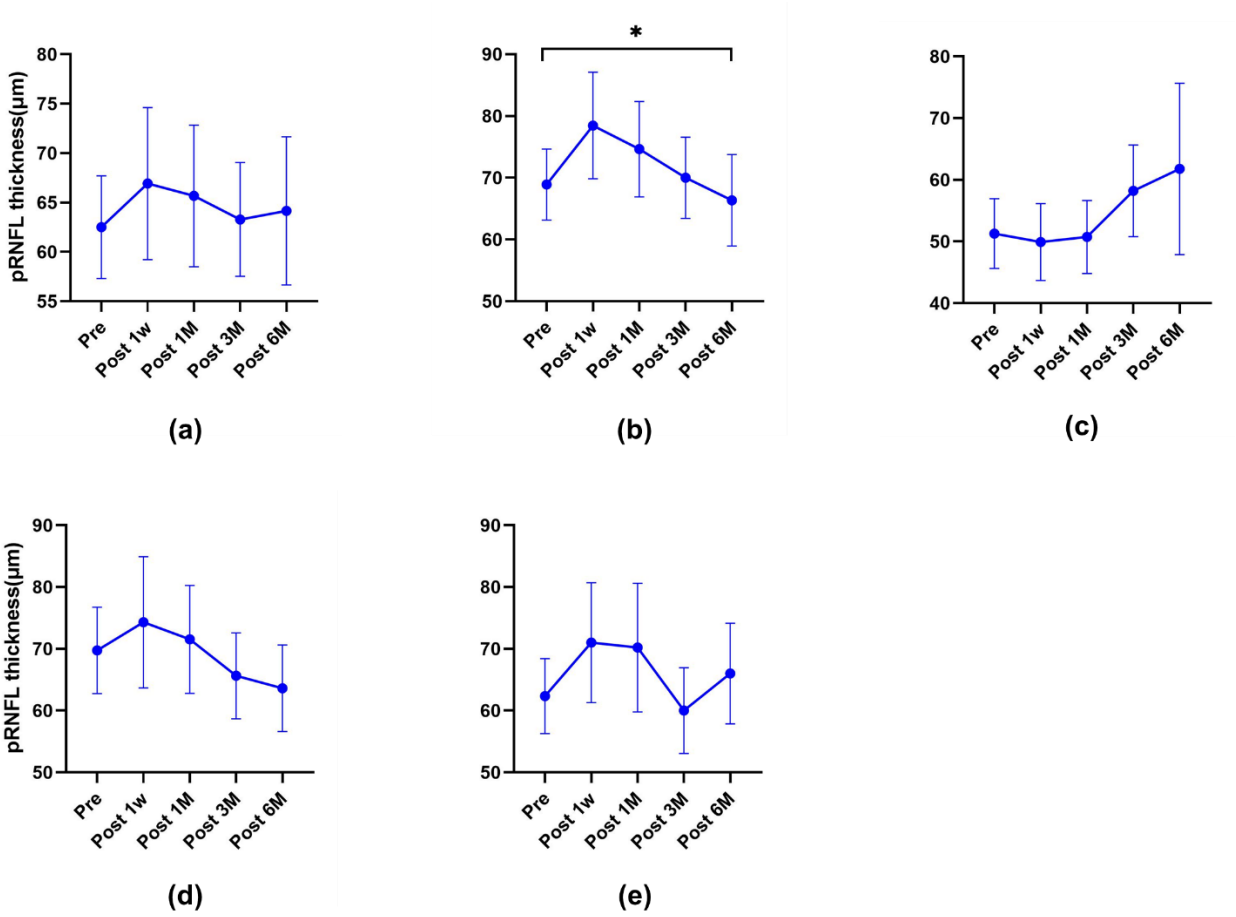


**Figure 15:** Average RNFL thickness in the peripapillary subregions. (a) Average RNFL thickness across the entire peripapillary region (b) Inferior region (c) Nasal region (d) Superior region (e) Temporal region

## 3.4 Analysis of IOP and VD Parameters

Postoperative IOP showed a gradual decline throughout the follow-up period. IOP showed a significant reduction over time. The preoperative mean IOP was 22.26 ± 7.66 mmHg, which decreased to 18.5 ± 9.56 mmHg at one week ($p = 0.058$) and significantly declined to 15.46 ± 5.29 mmHg at one month ($p = 0.029$). The reduction continued to 13.86 ± 7.29 mmHg at three months ($p = 0.034$) and reached 12.01 ± 2.10 mmHg at six months ($p = 0.005$) (Figure 16).

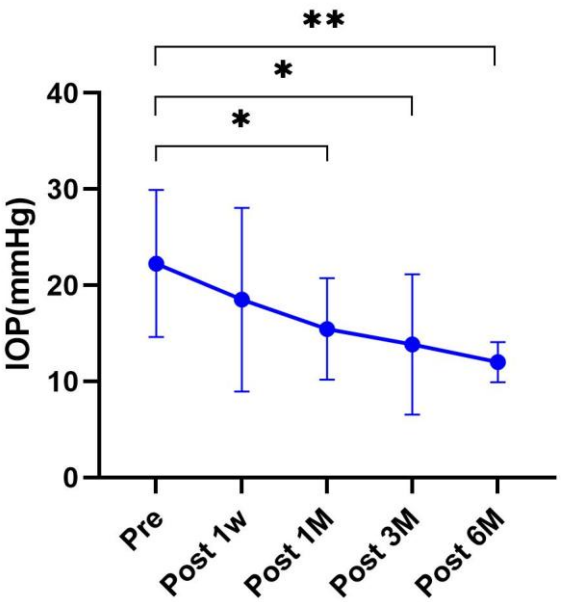


**Figure 16:** IOP Changes from Baseline up to 6 Months Postoperatively

In the visual field examination, we extracted preoperative and six-month postoperative data for visual field index (VFI), MD, and PSD. The VFI decreased from 0.667±0.297 preoperatively to 0.599±0.310 at six months post-surgery. The preoperative MD decreased from -12.49±14.30 dB to -15.83±10.59 dB at six months post-surgery. The preoperative PSD slightly increased from 7.944±3.617 to 8.03±3.917 at six months post-surgery. Although the changes in VFI, MD, and PSD were not statistically significant, the trends suggest a decline in VFI, an increase in the negative value of MD, and a slight increase in PSD, all of which indicate a potential deterioration in VF function(Figure 17).

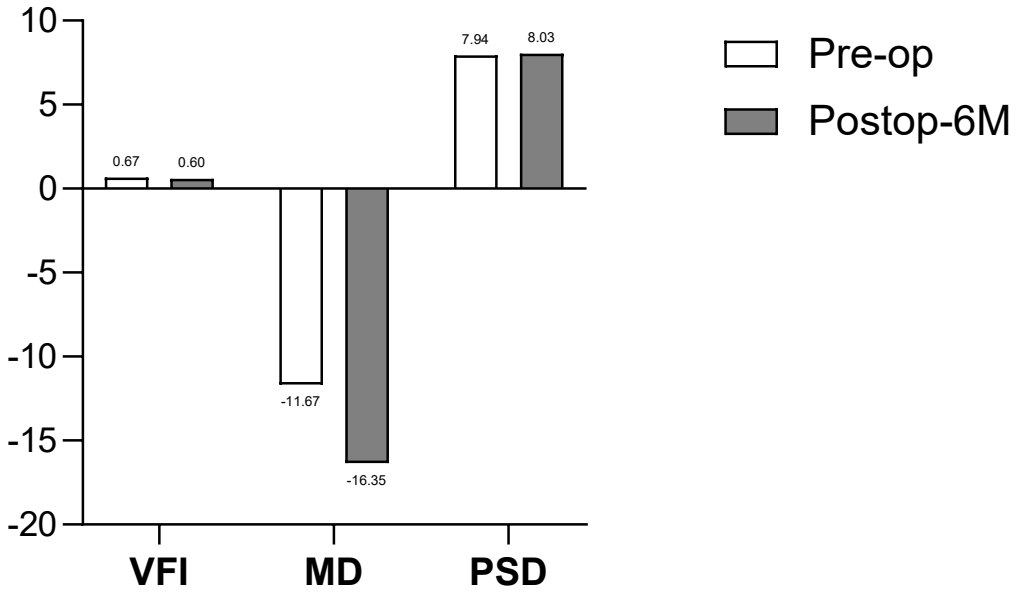


**Figure 17:** VF Parameters Changes from Baseline up to 6 Months Postoperatively

3.5 Linear Regression Analysis

We conducted a linear regression analysis by categorizing OCTA vascular density data into three groups based on different imaging areas: 3 mm × 3 mm macular, 6 mm × 6 mm macular, ONH and peripapillary. The aim was to identify factors associated with VD changes across different regions from the preoperative period to six months postoperatively. The core objective of the regression analysis was to investigate the impact of independent variables, such as age, IOP, mRNFL thickness, and pRNFL thickness, on VD as the dependent variable. Both univariate and multivariate analyses were performed; however, our primary focus was on the multivariate analysis. By incorporating multiple independent variables, the multivariate analysis provides a more comprehensive assessment, offering more accurate conclusions based on the interactions among various factors.

3.5.1 3 mm × 3 mm Macular Region

**Table 2:** Linear Regression Analysis on the VD in Subregions of 3 mm × 3 mm Macular Imaging

| 3×3 Macula | | Fovea(pValue) | | Inferior(pValue) | | Nasal(pValue) | | Superior(pValue) | | Temporal(pValue) | |
|---|---|---|---|---|---|---|---|---|---|---|---|
| | | Univariate | Multivariate | Univariate | Multivariate | Univariate | Multivariate | Univariate | Multivariate | Univariate | Multivariate |
| ***IOP*** | | 0.786 | | 0.947 | | 0.302 | 0.328 | 0.871 | 0.726 | 0.621 | 0.173 |
| ***MD*** | | 0.818 | | 0.729 | 0.315 | 0.599 | 0.744 | 0.864 | 0.224 | 0.451 | 0.305 |
| ***Age*** | | 0.067 | 0.134 | **0.002** | | **<0.001** | 0.166 | **0.014** | 0.206 | 0.09 | 0.073 |
| ***ONH*** | ***G*** | **0.036** | | 0.884 | | 0.442 | | 0.72 | | 0.618 | |
| | ***I*** | 0.128 | 0.226 | 0.946 | 0.147 | 0.254 | 0.224 | 0.745 | 0.25 | 0.733 | 0.721 |
| | ***N*** | 0.126 | 0.082 | 0.639 | 0.063 | 0.842 | 0.324 | 0.989 | 0.157 | 0.683 | **0.028** |
| | ***S*** | 0.327 | **0.027** | 0.398 | **0.032** | 0.803 | **0.027** | 0.374 | **0.036** | 0.265 | 0.265 |
| | ***T*** | **0.005** | **0.044** | 0.494 | 0.835 | 0.102 | **0.011** | 0.569 | 0.075 | 0.833 | 0.072 |
| ***Macula*** | ***F*** | 0.287 | **0.001** | 0.395 | 0.557 | 0.829 | **0.036** | 0.445 | **0.047** | 0.898 | **0.001** |
| | ***I*** | 0.396 | 0.058 | 0.378 | 0.61 | 0.381 | 0.447 | 0.75 | 0.377 | 0.97 | 0.053 |
| | ***N*** | 0.412 | 0.441 | 0.804 | 0.288 | 0.16 | 0.134 | 0.375 | 0.7 | 0.948 | 0.736 |
| | ***S*** | 0.092 | 0.89 | 0.406 | **0.022** | 0.988 | 0.846 | 0.533 | 0.244 | 0.491 | 0.063 |
| | ***T*** | 0.954 | **0.023** | 0.232 | 0.771 | 0.798 | 0.37 | 0.621 | 0.324 | 0.777 | **0.011** |
| ***Followup*** | | | 0.224 | | **0.043** | | 0.588 | | 0.079 | | **0.004** |
| ***Fazperi*** | | 0.552 | **<0.001** | 0.509 | 0.322 | 0.923 | **0.001** | **0.041** | 0.682 | 0.566 | 0.682 |
| ***FAZarea*** | | **<0.001** | **<0.001** | **0.014** | 0.262 | 0.062 | **0.006** | **0.004** | **0.038** | 0.083 | **0.038** |

We performed a linear regression analysis on the vessel density in different subregions of the 3 mm × 3 mm macular imaging. In the Fovea region, vascular density showed significant associations in the multivariate analysis with pRNFL thickness in the Superior (p=0.027) and Temporal (p=0.044) regions, mRNFL thickness in the Fovea (p=0.001) and Temporal (p=0.023) regions, as well as the FAZ perimeter (p<0.001) and FAZ area (p<0.001)(Table 2).

In the Inferior region, vascular density was significantly associated with pRNFL thickness in the Superior region (p=0.032), mRNFL thickness in the superior region (p=0.022), and follow-up time (p=0.043) in the multivariate analysis (Table 2).

In the nasal region, VD showed significant associations in the multivariate analysis with pRNFL thickness in the superior (p=0.027) and temporal (p=0.011) regions, mRNFL thickness in the fovea region (p=0.036), as well as the FAZ perimeter (p=0.001) and FAZ area (p=0.006)(Table 2).

In the superior region, VD was significantly associated in the multivariate analysis with pRNFL thickness in the superior region (p=0.036), mRNFL thickness in the fovea region (p=0.047), and the FAZ area (p=0.038) (Table 2).

In the temporal region, VD showed significant associations in the multivariate analysis with pRNFL thickness in the nasal region (p=0.028), mRNFL thickness in the fovea (p=0.001) and temporal (p=0.011) regions, follow-up time (p=0.004), and the FAZ area (p=0.038)(Table 2).

3.5.2 6 mm × 6 mm Macular Region

**Table 3:** Linear Regression Analysis on the VD in Subregions of 6 mm × 6 mm Macular Imaging

| **6×6 Macula** | | **Inferior(pValue)** | | **Nasal(pValue)** | | **Superior(pValue)** | | **Temporal(pValue)** | |
|---|---|---|---|---|---|---|---|---|---|
| | | Univariate | Multivariate | Univariate | Multivariate | Univariate | Multivariate | Univariate | Multivariate |
| ***IOP*** | | 0.428 | 0.561 | 0.218 | 0.312 | 0.427 | 0.993 | 0.928 | 0.479 |
| ***MD*** | | 0.741 | 0.316 | 0.46 | 0.07 | 0.174 | 0.404 | 0.51 | 0.939 |
| ***Age*** | | 0.321 | 0.832 | 0.434 | 0.176 | 0.829 | 0.547 | 0.311 | 0.209 |
| ***ONH*** | ***G*** | 0.078 | 0.964 | **0.003** | 0.602 | **0.021** | 0.443 | **0.039** | 0.423 |
| | ***I*** | **0.004** | 0.871 | **<0.001** | 0.47 | **0.014** | 0.299 | **0.036** | 0.528 |
| | ***N*** | 0.918 | 0.869 | 0.9 | 0.776 | 0.293 | 0.537 | 0.22 | 0.443 |
| | ***S*** | 0.195 | 0.951 | **0.005** | 0.623 | **0.004** | 0.437 | **0.006** | 0.804 |
| | ***T*** | **0.009** | 0.796 | **<0.001** | 0.345 | 0.076 | 0.485 | 0.252 | 0.282 |
| ***Macula*** | ***F*** | 0.32 | 0.634 | **0.004** | 0.142 | 0.732 | 0.103 | 0.594 | 0.36 |
| | ***I*** | 0.364 | 0.974 | **0.002** | 0.782 | 0.267 | **0.022** | 0.695 | 0.606 |
| | ***N*** | 0.253 | 0.441 | **<0.001** | 0.861 | 0.105 | 0.248 | 0.703 | 0.677 |
| | ***S*** | 0.961 | 0.946 | 0.094 | 0.831 | **0.005** | **0.01** | 0.479 | 0.118 |
| | ***T*** | 0.484 | 0.881 | **0.003** | 0.857 | 0.605 | **0.01** | 0.407 | 0.525 |
| ***Followup*** | | | 0.59 | | **0.045** | | **0.02** | | 0.342 |
| ***Fazperi*** | | 0.502 | 0.247 | 0.212 | 0.302 | 0.713 | 0.901 | 0.066 | 0.624 |
| ***FAZarea*** | | 0.712 | 0.836 | 0.318 | 0.399 | 0.807 | 0.735 | **0.022** | 0.126 |

We performed a linear regression analysis on the vascular density in different subregions of the 6 mm × 6 mm macular imaging(Table 3).

In the inferior region, VD showed a significant univariate association with pRNFL thickness in the inferior (p=0.004) and temporal (p=0.009) regions. However, no significant associations were identified in the multivariate analysis (Table 3).

In the nasal region, VD was significantly associated with follow-up time (p=0.045) in the multivariate analysis (Table 3).

In the superior region, VD demonstrated significant associations in the multivariate analysis with mRNFL thickness in the inferior (p=0.022), superior (p=0.01), and temporal (p=0.02) regions, as well as follow-up time (p=0.02) (Table 3).

In the temporal region, VD showed significant univariate associations with pRNFL thickness in certain regions and FAZ area. However, no significant associations were identified in the multivariate analysis (Table 3).

3.5.3 ONH and Peripapillary Region

**Table 4:** Linear Regression Analysis on the VD in Subregions of ONH and Peripapillary Imaging

| **Peripapillary Region** | | **optic disc(pValue)** | | **Inferior(pValue)** | | **Nasal(pValue)** | | **Superior(pValue)** | | **Temporal(pValue)** | |
|---|---|---|---|---|---|---|---|---|---|---|---|
| | | Univariate | Multivariate | Univariate | Multivariate | Univariate | Multivariate | Univariate | Multivariate | Univariate | Multivariate |
| ***IOP*** | | 0.06 | 0.51 | 0.685 | 0.637 | 0.833 | 0.911 | 0.709 | 0.374 | 0.27 | 0.858 |
| ***MD*** | | 0.129 | 0.544 | 0.946 | 0.786 | 0.434 | 0.269 | 0.145 | 0.627 | 0.842 | 0.914 |
| ***Age*** | | 0.122 | 0.116 | **<0.001** | **0.002** | **0.037** | 0.093 | 0.161 | 0.33 | **<0.001** | **<0.001** |
| ***ONH*** | ***G*** | **<0.001** | 0.62 | **<0.001** | | 0.316 | --- | **0.006** | --- | 0.19 | --- |
| | ***I*** | **<0.001** | 0.513 | **<0.001** | 0.488 | 0.188 | 0.088 | **0.036** | 0.41 | 0.245 | 0.248 |
| | ***N*** | **0.002** | --- | 0.071 | 0.217 | **0.037** | 0.505 | 0.315 | 0.113 | 0.79 | 0.072 |
| | ***S*** | **<0.001** | 0.411 | **<0.001** | 0.92 | **0.043** | **0.019** | **<0.001** | 0.23 | 0.269 | 0.276 |
| | ***T*** | **<0.001** | 0.931 | **<0.001** | 0.112 | 0.962 | 0.505 | **0.003** | 0.5 | **0.035** | 0.544 |
| ***Macula*** | ***F*** | **0.001** | 0.805 | 0.25 | --- | 0.886 | 0.656 | **0.05** | 0.469 | 0.397 | 0.971 |
| | ***I*** | **0.008** | 0.812 | 0.08 | 0.947 | 0.331 | 0.202 | **0.042** | --- | 0.356 | --- |
| | ***N*** | **<0.001** | 0.189 | **0.009** | 0.778 | 0.994 | 0.995 | **0.005** | 0.307 | 0.074 | 0.58 |
| | ***S*** | **0.007** | 0.513 | 0.65 | 0.978 | 0.097 | 0.994 | **0.003** | 0.37 | 0.768 | 0.463 |
| | ***T*** | **0.024** | 0.596 | 0.375 | | 0.305 | 0.356 | 0.101 | | 0.82 | 0.42 |
| ***Followup*** | | | 0.14 | | 0.617 | | 0.152 | | 0.626 | | 0.253 |
| ***Fazperi*** | | **0.044** | 0.226 | 0.931 | 0.202 | **0.002** | **0.022** | 0.169 | 0.889 | 0.284 | 0.838 |
| ***FAZarea*** | | 0.205 | 0.938 | 0.108 | 0.092 | 0.085 | 0.573 | **0.032** | 0.214 | **0.015** | 0.176 |

We performed a linear regression analysis on the vascular density in different subregions of the ONH and peripapillary OCTA imaging (Table 4).

Although VD in the optic disc and superior regions showed significant univariate associations with macular and peripapillary RNFL thickness, no significant associations were identified in the multivariate analysis (Table 4).

In the Inferior and temporal regions, VD was significantly associated with age (p=0.002) in the multivariate analysis (Table 4).

In the nasal region, VD showed significant associations in the multivariate analysis with pRNFL thickness in the superior region (p=0.019) and FAZ perimeter (p=0.022) (Table 4).

In this study, we performed a linear regression analysis to investigate the associations between vascular density in the 3 mm × 3 mm macular region and various independent variables. The results demonstrated that VD in this region showed the highest number of significant multivariate associations, far exceeding those observed in the 6 mm × 6 mm macular and peripapillary regions. This finding suggests that VD in the 3 mm × 3 mm macular region may be more sensitive to the studied independent variables or that vascular changes in this region are influenced by a greater number of factors. Compared to the broader 6 mm × 6 mm macular and peripapillary regions, VD in the 3 mm × 3 mm macular region may be more representative and valuable for analysis, particularly in studies focusing on subtle microvascular changes.

# 4 Discussion

## 4.1 Main Findings

This study primarily evaluated the dynamic changes in optic disc, peripapillary and macular VD, FAZ parameters, and macular and peripapillary RNFL thickness in glaucoma patients following PGI surgery over a 6-month follow-up period. The results revealed that, in the macular region, the VD of the parafovea and fovea showed a transient decrease one week post-surgery, with no statistically significant changes. Subsequently, a peak in VD increase was observed between one and three months post-surgery, with statistically significant changes in some areas, particularly in the fovea and temporal regions. However, the VD in the fovea region slightly decreased towards baseline levels by the 6-month follow-up, while the temporal region maintained a significant increase at 6 months. The VD of the perifovea continued to fluctuate over the 6-month follow-up, and the full retinal VD showed an increase at 6 months compared to baseline, but this change was not statistically significant.

The VD of the optic disc and peripapillary region decreased between one and three months post-surgery, but by six months, most regions showed an increase. Except for the NI and ST regions, the retinal VD at six months post-surgery was higher than the baseline VD, though this change was not statistically significant. FAZ area and perimeter reached their minimum values at three months post-surgery, with statistically significant changes, indicating improved central macular perfusion post-surgery. The RNFL thickness surrounding the macula and peripapillary generally decreased and then returned to baseline values, with a transient increase in RNFL thickness observed one-week post-surgery. Only the inferior region of the peripapillary region showed a statistically significant decrease in RNFL thickness. Linear regression analysis revealed significant multifactorial linear correlations between age, follow-up time, FAZ perimeter and area, and RNFL thickness in the macular and peripapillary regions with VD.

## 4.2 Changes in Retinal VD and Implications

The short-term postoperative increase in VD observed in this study is likely attributable to the improvement in ocular perfusion pressure (OPP) following the reduction in IOP after PGI surgery. IOP significantly decreased postoperatively, and the need for anti-glaucoma medications was markedly reduced, potentially mitigating vasoconstrictive effects induced by topical agents. In our study, the superficial and deep capillary plexus VD in the foveal and parafoveal regions initially decreased at postoperative week 1, followed by a gradual increase, peaking at 3 months. Notably, significant changes were observed in the foveal and temporal subregions, suggesting that these areas may be more sensitive to perfusion improvements.

The transient VD reduction at week 1 aligns with the findings of Jung et al., who used OCTA to evaluate peripapillary and optic disc VD changes in glaucoma patients after trabeculectomy (In et al., 2018). They reported a slight decrease in peripapillary VD at postoperative week 1, followed by a progressive increase thereafter. A possible explanation is that the significant IOP reduction observed at week 1 may induce changes in axial length. Previous studies have indicated that postoperative IOP reduction can shorten axial length, which in turn is negatively correlated with retinal VD (Francis et al., 2005; Kook et al., 2001; Huang et al., 2024; Chen et al., 2023). Sampson et al. demonstrated that axial length changes can affect measurements of superficial retinal VD and FAZ area in OCTA (Sampson et al., 2017). Without proper correction, these parameters may be subject to considerable measurement errors. In our study, the transient decrease in retinal VD at week 1 may partly reflect such axial length-induced imaging artifacts.

Although VD remained significantly increased at 1 and 3 months postoperatively, by 6 months only the deep parafoveal temporal region retained statistical significance, while other regions showed no significant differences compared to baseline. Interestingly, most regions exhibited a peak in VD at 3 months, followed by a slight decline and subsequent stabilization by 6 months. These findings are consistent with the study by Ch’ng et al., who reported that foveal VD began to decline one month postoperatively, increased steadily by 6 months, and then slightly decreased again at 12 months (Ch'ng et al., 2020). Similar trends were observed in the parafoveal and perifoveal regions, although the changes in those areas did not reach statistical significance.

This temporal pattern may reflect a new hemodynamic equilibrium reached after initial improvements in ocular perfusion in the posterior segment. Several studies have shown that vascular autoregulation is impaired in glaucoma patients, potentially resulting in a delayed vascular response to IOP changes—characterized by VD increase at 1–3 months postoperatively and partial regression by 6 months (Fuchsjäger-Mayrl et al., 2004; Luo et al., 2015; Pillunat et al., 1987; Hwang et al., 2012). Patel et al. investigated the effects of IOP fluctuations on ONH structure and vasculature in healthy non-human primates and found that peripapillary VD decreased significantly only when IOP exceeded 50 mmHg, and rapidly recovered when IOP returned below 40 mmHg (Patel et al., 2018). Their findings suggest that in healthy vasculature, VD changes in OCTA become significant only beyond a certain IOP threshold. Nonetheless, this also underscores that retinal VD in early glaucoma may indeed be susceptible to IOP fluctuations, particularly when intervention is timely.

In the ONH and peripapillary region, a general trend of increased VD was observed over the 6-month postoperative period, but the changes were not statistically significant. This suggests that ONH and peripapillary perfusion may not consistently improve despite significant IOP reduction. Our findings align with previous studies; for instance, Ch'ng et al. reported considerable fluctuations in peripapillary VD throughout follow-up, with only NI and IT sectors showing statistically significant changes (Ch'ng et al., 2020). Zéboulon et al. also found minimal overall changes in VD following glaucoma surgery, with significant differences only in the inferior macular subregion in some patients (Zéboulon et al., 2017). Conversely, Holló et al. demonstrated an increase in peripapillary blood flow density in all cases after substantial IOP reduction in high-pressure glaucoma patients (Holló, 2017). Notably, in their study, baseline IOP ranged from 35–42 mmHg and decreased to 12–18 mmHg after treatment—a reduction of 17–30 mmHg.

In contrast, the baseline IOP in our cohort was 22.26 ± 7.66 mmHg, and the final postoperative IOP at the last follow-up averaged 12.01 ± 2.10 mmHg, reflecting a smaller overall reduction. Previous studies have shown that perfusion impairment in the ONH may occur early in glaucoma, indicating that irreversible vascular degeneration may have already taken place before surgery (Fuchsjäger-Mayrl et al., 2004; Shiga et al., 2016; Shiga et al., 2013). Chronic IOP elevation can also impair autoregulatory mechanisms in

ONH microcirculation, compounding vascular dysregulation (Wang et al., 2014). In our study, although IOP significantly declined postoperatively, ONH and peripapillary region VD did not exhibit meaningful recovery by 6 months, and even decreased in some regions. This may reflect the slow nature of ONH and peripapillary vascular restoration or the presence of substantial preexisting structural vascular damage.

A notable feature of our study population is that most patients presented with advanced disease: 75 % had undergone previous anti-glaucoma surgeries before Paul tube implantation, and the average number of anti-glaucoma medications used preoperatively exceeded three. Long-standing high IOP may have led to irreversible perfusion injury and impaired vascular reactivity, thereby limiting postoperative VD recovery in ONH and peripapillary.

### 4.3 Dynamic Changes in FAZ and Their Clinical Significance

The FAZ reflects the microcirculatory status of the central macula. In our study, both FAZ area and perimeter reached their lowest values at 3 months postoperatively, with statistically significant changes. This finding is consistent with Shoji et al. and Park et al., who also reported postoperative FAZ shrinkage in both superficial and deep capillary layers (Shoji et al., 2022; Park et al., 2021). Given that the FAZ lacks intrinsic capillaries, its boundary perfusion is particularly sensitive to changes in perfusion pressure. The observed postoperative FAZ reduction thus likely reflects improved macular perfusion and suggests its utility as an indirect marker of microcirculatory recovery following glaucoma interventions.

Furthermore, Ch’ng et al. observed a similar trend, with early postoperative FAZ shrinkage that gradually returned to near-baseline values by 12 months (Ch'ng et al., 2020). This is consistent with our observation that while FAZ area and perimeter remained slightly smaller than baseline at 6 months, they had already increased from the 3-month minimum, suggesting a gradual reversion to baseline. It is therefore reasonable to speculate that with extended follow-up to 12 months, FAZ parameters might further approximate or return to preoperative levels.

### 4.4 Interpretation of Other Results

### 4.4.1 Changes in RNFL Thickness

In both the macular and peripapillary regions, RNFL thickness exhibited a transient increase at one week postoperatively, followed by a decreasing trend over time, returning to baseline levels by six months after surgery. The decrease was particularly significant in the inferior sector of the peripapillary region. These findings are consistent with previous studies. Raghu et al. observed a significant increase in RNFL thickness at one week postoperatively, which returned to preoperative values by three months (Raghu et al., 2012). Similarly, Ch'ng et al. reported a transient increase in RNFL thickness within the first month after filtration surgery (Ch'ng et al., 2020). In contrast, Gillmann et al. did not observe such an increase at one week following laser trabeculoplasty, which differs from our findings (Gillmann et al., 2022). This discrepancy may be attributed to postoperative inflammation, which is considered one of the potential causes of increased RNFL thickness. Our study shares greater similarity in surgical approach with Raghu et al. (trabeculectomy) and Ch'ng et al. (predominantly deep sclerectomy), whereas Gillmann et al. investigated a less invasive procedure—laser trabeculoplasty—which likely induces less ocular inflammation (Raghu et al., 2012; Ch'ng et al., 2020). Some studies have shown that the IOP reduction of trabeculoplasty may exhibit a slow response, with a significant decrease in IOP occurring between 4 to 12 weeks postoperatively (Keyser et al., 2017; Nagar et al., 2009). Moreover, the magnitude of IOP reduction achieved by trabeculoplasty is generally less than penetrating glaucoma surgeries, such as trabeculectomy. Although previous researches have indicated that a transient increase of RNFL thickness is associated with IOP reduction, we still consider postoperative inflammation to be the primary cause of the increased RNFL thickness (Weigert et al., 2005). The inflammatory response following surgery, along with tissue injury during the procedure, may lead to increased production of free radical and the release of growth factors and prostaglandins, all of which can contribute to postoperative thickening of RNFL (Anderson et al., 2002; Fakhraie et al., 2019; Pollack et al., 1996).

### 4.4.2 Changes in IOP, BCVA, and VF Parameters

In this study, IOP demonstrated a significant decreasing trend at all postoperative time points, indicating that the Paul tube implantation effectively achieved IOP control within the 6-month follow-up period. This finding is consistent with previous studies on the IOP-

lowering efficacy of glaucoma drainage devices and lays a foundation for subsequent improvements in retinal perfusion and structural changes (Labay-Tejado et al., 2024; Vallabh et al., 2023; Tan et al., 2024). The reduction in IOP is considered a prerequisite for enhancing fundus perfusion and delaying microvascular degeneration in the macula and optic disc, and also serves as a key external factor influencing changes in VD (Mahmoudinezhad et al., 2024; Du et al., 2020).

Although this study did not primarily focus on functional visual improvement, changes in BCVA were nonetheless recorded during the 6-month follow-up. Given that the study population consisted predominantly of glaucoma patients rather than individuals with macular diseases, the limited improvement in visual acuity was anticipated. This outcome suggests that BCVA may not serve as a sensitive indicator for detecting microvascular perfusion or structural alterations in short-term follow-up among glaucoma patients.

Visual field parameters, including MD and PSD, showed no statistically significant changes, but the overall data suggested a potential worsening of the VF function. This result aligns with previous reports indicating that, even under well-controlled postoperative IOP, visual function in glaucoma patients may continue to deteriorate gradually over time. (Weber et al., 2024; Weber et al., 2023). Although current evidence regarding postoperative VF changes following PGI surgery is limited, findings from studies on other types of drainage procedures similarly suggested that postoperative VF indices, such as MD, exhibit gradual deterioration. (Wagner et al., 2020; Schargus et al., 2020; Junoy Montolio et al., 2019). This phenomenon may be attributed to the irreversible nature of glaucomatous VF loss and its typically slow progression.

### 4.5 Interpretation of Linear Regression Analysis Results

To further explore the factors influencing VD, this study constructed a linear regression model with VD in the ONH, peripapillary region and macular as dependent variables and age, IOP, mRNFL thickness, and pRNFL thickness as independent variables. The results showed that age, follow-up time, FAZ perimeter and area, and macular and pRNFL thickness were significantly correlated with VD in a multifactorial linear relationship. The FAZ perimeter and area were negatively correlated with the parafoveal and peripapillary VD, which aligns with the hypothesis that improved perfusion occurs as FAZ reduces.

Parafoveal and perifoveal VD were positively correlated with RNFL thickness in most sectors of the macula and peripapillary region, suggesting that individuals with more intact macular structures exhibit better perfusion.

Notably, only the superior sector of the peripapillary area showed a positive correlation with peripapillary VD, indicating that the perfusion recovery in the ONH and peripapillary region may be influenced by multiple factors. This finding is consistent with previous studies. In et al. demonstrated in their multivariate linear regression analysis that the rebound of peripapillary VD was not significantly correlated with RNFL thickness or IOP (In et al., 2018). Other studies have suggested that the improvement in ONH perfusion is influenced by various biomechanical factors and structural changes (Shin et al., 2017; Kim et al., 2018). Preoperative and postoperative IOP and MD values were not correlated with VD, suggesting that VD changes are not solely driven by IOP or visual function. This finding is consistent with previous studies (Shin et al., 2017; In et al., 2018). Park et al. reported that in some patients, despite successful IOP reduction after surgery, VD did not change or even showed a reverse trend (Park et al., 2021). These results support the notion that VD is influenced by multiple factors, indicating a complex and dynamic relationship between perfusion, structure, and function.

The changes in VD should be understood as the cumulative result of the interaction between structure, function, and perfusion, rather than solely driven by IOP or RNFL thickness changes. On the one hand, IOP reduction can improve local blood flow by increasing OPP, thereby enhancing VD (Wang et al., 2020; Holló, 2017). On the other hand, if irreversible retinal damage has occurred (manifesting as RNFL thinning), the demand for perfusion decreases, and even if perfusion pressure improves, the blood flow network may continue to degenerate due to the "loss of blood supply targets." Meanwhile, VD changes are closely related to visual function status. Previous studies have found a positive correlation between the degree of visual field loss (e.g., MD decrease) and local VD, suggesting that areas with functional damage often exhibit reduced perfusion, which may result from ischemic changes due to prolonged low perfusion or reflect a reduction in blood flow after decreased metabolic demand in those regions (Lin et al., 2020; Zhong et al., 2022; Yarmohammadi et al., 2016). Previous research has also indicated that VF damage is related to reduced retinal blood flow and structural loss in the RNFL and

peripapillary region (Hwang et al., 2012). Therefore, dynamic changes in VD should not be isolated as an indicator of IOP control efficacy but should be considered in conjunction with the interaction balance between the integrity of neuro-structural tissue, visual function status, and perfusion regulation capacity.

Interestingly, we observed that the parafoveal region exhibited the most significant changes in VD in the OCTA results, showing the strongest statistical significance in the comparisons of VD at follow-up time points. In the subsequent linear regression analysis, VD in this region was also significantly correlated with the most independent variables, significantly surpassing the perifoveal and peripapillary regions in terms of OCTA metrics. This trend suggests that parafoveal VD may be more sensitive to intraocular and systemic physiological parameters or may be more easily influenced by the combined effects of multiple factors during postoperative perfusion regulation (Resch et al., 2021; Kim et al., 2021).

In comparison to the 6 mm × 6 mm macula scan, which covers a larger field of view, the 3 mm × 3 mm region provides higher resolution and finer microvascular presentation, making it more likely to capture early or subtle perfusion changes in the postoperative period. Furthermore, as the parafoveal region includes the central fovea and the dense capillary network surrounding it, it may more effectively reflect the dynamic relationship between local structure, perfusion, and function. Therefore, in evaluating the sensitivity and representativeness of postoperative microvascular changes, parafoveal VD may have higher analytical value.

### 4.6 Clinical Implications and Limitations of the Study

The results of this study suggest that early vascular density in the macular region can be significantly improved after Paul tube implantation, especially in the fovea and temporal regions, with FAZ showing signs of enhanced perfusion. Combined with reductions in IOP and medication use, postoperative OCTA parameters may serve as valuable tools for early monitoring of therapeutic effects, helping to assess improvements in perfusion and disease control outcomes.

However, this study has several limitations. First, the sample size is limited, and the results should be verified in a larger cohort. Second, the 6-month follow-up may not be sufficient to reveal long-term microcirculation trends, as several studies have shown that VD continues to change up to 12 months after intervention (Ch'ng et al., 2020; Song et al., 2021). Third, since 75 % of the patients included in this study had undergone other glaucoma surgeries before PGI surgery, and some patients had retinal vascular diseases, the changes in VD may be influenced by various patient-specific factors, potentially affecting the statistical results. Additionally, 35 % of patients still required glaucoma medications postoperatively. Studies have demonstrated that glaucoma medications can also affect ocular blood flow, which may further influence changes in retinal vascular density (Feke et al., 2014; Tsuda et al., 2013; Reber et al., 2003; Siesky et al., 2009). Future studies could consider narrowing patient inclusion criteria, extending follow-up periods, and incorporating multimodal analyses such as functional-perfusion combined imaging to explore the interactive mechanisms between structure, function, and perfusion on VD changes more thoroughly.

# 5 Summary

This study aimed to evaluate the changes in VD and associated retinal structural parameters in the macular and optic disc regions during the follow-up period after PGI using OCTA imaging. Furthermore, it sought to investigate the potential mechanisms of intraocular perfusion regulation and its relationship with structure and function, as well as analyzing the correlation between VD changes and systemic and intraocular physiological parameters in patients.

Patients with glaucoma who underwent PGI were included in this study. VD changes in the macular and peripapillary regions were assessed using 3×3 mm and 6×6 mm OCTA scans. Additional parameters, including RNFL thickness, FAZ area and perimeter, visual function (MD and PSD), as well as preoperative and postoperative IOP, were collected over a 6-month follow-up period. A linear regression analyses were performed to explore the associations between VD and related factors, aiming to elucidate the sensitivity of VD in different regions to local perfusion regulation.

Results: During the postoperative follow-up period, VD in the macular region showed a significant overall increase, whereas VD changes in the optic disc region were more complex, with limited improvement or even slight decreases in certain areas. Among the macular subregions, the parafoveal region demonstrated the most pronounced changes in VD. Both intertemporal comparisons and linear regression analyses revealed that parafoveal VD exhibited statistically significant correlations with the largest number of independent variables, surpassing the perifoveal region as well as the ONH and peripapillary regions. The high-resolution 3×3 mm scan proved to be more sensitive in detecting subtle postoperative perfusion changes, particularly in reflecting the perfusion dynamics of the fovea and its surrounding dense capillary network. The FAZ area and perimeter were significantly reduced at 3 months postoperatively, indicating improved macular perfusion. By 6 months, partial recovery was observed, but values remained below baseline levels, suggesting a prolonged adjustment process of macular perfusion following surgery. RNFL thickness exhibited a transient increase at 1 week postoperatively, likely related to the release of free radicals, growth factors, and prostaglandins triggered

by inflammatory responses. By the 6-month follow-up, RNFL thickness had returned to baseline levels, with slight fluctuations observed in certain regions. Postoperative IOP decreased significantly and remained consistently lower than baseline levels across all follow-up time points. However, visual function parameters, such as MD and PSD, showed no significant improvement. Data from some patients suggested a gradual progression of visual field defects, consistent with the irreversible and slowly progressive nature of glaucomatous damage.

After PGI, VD in the macular region significantly increased postoperatively, while changes in the ONH and peripapillary region were more complex, with limited improvement or slight decreases in some sub regions. We observed that parafoveal VD is more sensitive to dynamic intraocular perfusion regulation, highlighting its significant clinical analytical value. OCTA imaging effectively captures postoperative retinal microvascular changes, providing crucial insights into perfusion status and the structure-function relationship. Future studies with extended follow-up durations and multi-center designs are needed to further investigate the long-term effects of postoperative microvascular changes in the fundus.

# 6 List of figures

# 7 List of tables

# 8 References

Ahmad F, Deshmukh N, Webel A, Johnson S, Suleiman A, Mohan RR, Fraunfelder F, Singh PK. Viral infections and pathogenesis of glaucoma: a comprehensive review. Clinical Microbiology Reviews 2023; 36: e0005723

Allison K, Patel D, Alabi O. Epidemiology of Glaucoma: The Past, Present, and Predictions for the Future. Cureus; 12: e11686

Almousa R, Lake DB. Intraocular pressure control with Ahmed glaucoma drainage device in patients with cicatricial ocular surface disease-associated or aniridia-related glaucoma. International ophthalmology 2014; 34: 753–760

Anderson DH, Mullins RF, Hageman GS, Johnson LV. A role for local inflammation in the formation of drusen in the aging eye. American Journal of Ophthalmology 2002; 134: 411–431

Arora KS, Robin AL, Corcoran KJ, Corcoran SL, Ramulu PY. Use of Various Glaucoma Surgeries and Procedures in Medicare Beneficiaries from 1994 to 2012. Ophthalmology 2015; 122: 1615–1624

Bazvand F, Mirshahi R, Fadakar K, Faghihi H, Sabour S, Ghassemi F. The Quantitative Measurements of Vascular Density and Flow Area of Optic Nerve Head Using Optical Coherence Tomography Angiography. Journal of glaucoma 2017; 26: 735–741

Bell K, Rosignol I, Sierra-Filardi E, Rodriguez-Muela N, Schmelter C, Cecconi F, Grus F, Boya P. Age related retinal Ganglion cell susceptibility in context of autophagy deficiency. Cell Death Discovery 2020; 6: 1–13

Bogunjoko T, Hassan A, Ogunro A, Akanbi T, Ulaikere M, Ashaye A. Trends in glaucoma procedures and surgeries at the eye foundation hospital group, Nigeria. Nigerian journal of clinical practice 2019; 22: 1606–1610

Boland MV, Corcoran KJ, Lee AY. Changes in Performance of Glaucoma Surgeries 1994 through 2017 Based on Claims and Payment Data for United States Medicare Beneficiaries. Ophthalmology. Glaucoma 2021; 4: 463–471

Briers JD, Fercher AF. Retinal blood-flow visualization by means of laser speckle photography. Investigative ophthalmology & visual science 1982; 22: 255–259

Budenz DL, Barton K, Feuer WJ, Schiffman J, Costa VP, Godfrey DG, Buys YM. Treatment outcomes in the Ahmed Baerveldt Comparison Study after 1 year of follow-up. Ophthalmology 2011; 118: 443–452

Budenz DL, Barton K, Gedde SJ, Feuer WJ, Schiffman J, Costa VP, Godfrey DG, Buys YM. Five-year treatment outcomes in the Ahmed Baerveldt comparison study. Ophthalmology 2015; 122: 308–316

Camp DA, Yadav P, Dalvin LA, Shields CL. Glaucoma secondary to intraocular tumors: mechanisms and management. Current Opinion in Ophthalmology 2019; 30: 71–81

Cantor E, Méndez F, Rivera C, Castillo A, Martínez-Blanco A. Blood pressure, ocular perfusion pressure and open-angle glaucoma in patients with systemic hypertension. Clinical Ophthalmology (Auckland, N.Z.) 2018; 12: 1511–1517

Caprioli J. Glaucoma: A Disease of Early Cellular Senescence. Investigative ophthalmology & visual science 2013; 54: ORSF60-ORSF67

Carlo TE de, Romano A, Waheed NK, Duker JS. A review of optical coherence tomography angiography (OCTA). International journal of retina and vitreous 2015; 1: 5

Chakravarti T. Assessing Precision of Hodapp-Parrish-Anderson Criteria for Staging Early Glaucomatous Damage in an Ocular Hypertension Cohort: A Retrospective Study. Asia-Pacific journal of ophthalmology (Philadelphia, Pa.) 2017; 6: 21–27

Chang P-Y, Wang J-Y, Wang J-K, Huang T-L, Hsu Y-R. Optical Coherence Tomography Angiography Compared With Optical Coherence Tomography for Detection of Early Glaucoma With High Myopia. Frontiers in Medicine 2021; 8: 793786

Chen Y, Rong H, Liu Y, Gao H, Sun Z, Dang W, Lu K, Mi B, Li J, Wei R. Analysis of the relationship between axial length, optic disc morphology, and regional variations in retinal vessel density in young adults with healthy eyes. Frontiers in Medicine 2023; 10: 1280048

Ch'ng TW, Gillmann K, Hoskens K, Rao HL, Mermoud A, Mansouri K. Effect of surgical intraocular pressure lowering on retinal structures - nerve fibre layer, foveal avascular zone, peripapillary and macular vessel density: 1 year results. Eye 2020; 34: 562–571

Christakis PG, Zhang D, Budenz DL, Barton K, Tsai JC, Ahmed IIK. Five-Year Pooled Data Analysis of the Ahmed Baerveldt Comparison Study and the Ahmed Versus Baerveldt Study. American Journal of Ophthalmology 2017; 176: 118–126

Cicinelli MV, Rabiolo A, Sacconi R, Carnevali A, Querques L, Bandello F, Querques G. Optical coherence tomography angiography in dry age-related macular degeneration. Survey of Ophthalmology 2018; 63: 236–244

Coleman AL, Hill R, Wilson MR, Choplin N, Kotas-Neumann R, Tam M, Bacharach J, Panek WC. Initial clinical experience with the Ahmed Glaucoma Valve implant. American Journal of Ophthalmology 1995; 120: 23–31

D'Amico DJ. Diseases of the retina. The New England journal of medicine 1994; 331: 95–106

Davis BM, Crawley L, Pahlitzsch M, Javaid F, Cordeiro MF. Glaucoma: the retina and beyond. Acta Neuropathologica 2016; 132: 807–826

deLuise VP, Anderson DR. Primary infantile glaucoma (congenital glaucoma). Survey of Ophthalmology 1983; 28: 1–19

Di Zhao, Cho J, Kim MH, Guallar E. The association of blood pressure and primary open-angle glaucoma: a meta-analysis. American Journal of Ophthalmology 2014; 158: 615-627.e9

Du R, Wang X, Shen K, He S. Decreasing intraocular pressure significantly improves retinal vessel density, cytoarchitecture and visual function in rodent oxygen induced retinopathy. Science China. Life sciences 2020; 63: 290–300

Emre M, Orgül S, Haufschild T, Shaw SG, Flammer J. Increased plasma endothelin-1 levels in patients with progressive open angle glaucoma. The British Journal of Ophthalmology 2005; 89: 60–63

Fakhraie G, Mirghorbani M, Katz LJ, Mollazadeh A, Vahedian Z, Zarei R, Eslami Y, Mohammadi M, Hamzeh N, Masoomi A. Cystoid macular edema with prostaglandin analogue use after uneventful cataract surgery in glaucoma patients. Journal of cataract and refractive surgery 2019; 45: 1436–1445

Fechtner RD, Weinreb RN. Mechanisms of optic nerve damage in primary open angle glaucoma. Survey of Ophthalmology 1994; 39: 23–42

Feke GT, Bex PJ, Taylor CP, Rhee DJ, Turalba AV, Chen TC, Wand M, Pasquale LR. Effect of brimonidine on retinal vascular autoregulation and short-term visual function in normal tension glaucoma. American Journal of Ophthalmology 2014; 158: 105-112.e1

Fellman RL, Mattox C, Singh K, Flowers B, Francis BA, Robin AL, Butler MR, Shah MM, Giaconi JA, Sheybani A, Song BJ, Stein JD. American Glaucoma Society Position Paper: Microinvasive Glaucoma Surgery. Ophthalmology. Glaucoma 2020; 3: 1–6

Flammer J. The vascular concept of glaucoma. Survey of Ophthalmology 1994; 38 Suppl: S3-6

Flaxman SR, Bourne RRA, Resnikoff S, Ackland P, Braithwaite T, Cicinelli MV, Das A, Jonas JB, Keeffe J, Kempen JH, Leasher J, Limburg H, Naidoo K, Pesudovs K, Silvester A, Stevens GA, Tahhan N, Wong TY, Taylor HR, Vision Loss Expert Group of the Global Burden of Disease Study. Global causes of blindness and distance vision impairment 1990-2020: a systematic review and meta-analysis. The Lancet. Global Health 2017; 5: e1221-e1234

Francesco T de, Bacharach J, Smith O, Shah M. Early diagnostics and interventional glaucoma. Therapeutic Advances in Ophthalmology 2024; 16: 25158414241287431

Francis BA, Wang M, Lei H, Du LT, Minckler DS, Green RL, Roland C. Changes in axial length following trabeculectomy and glaucoma drainage device surgery. The British Journal of Ophthalmology 2005; 89: 17–20

François J, Laey JJ de. Fluorescein angiography of the glaucomatous disc. Ophthalmologica. Journal international d'ophtalmologie. International journal of ophthalmology. Zeitschrift fur Augenheilkunde 1974; 168: 288–298

Fuchsjäger-Mayrl G, Wally B, Georgopoulos M, Rainer G, Kircher K, Buehl W, Amoako-Mensah T, Eichler H-G, Vass C, Schmetterer L. Ocular blood flow and systemic blood pressure in patients with primary open-angle glaucoma and ocular hypertension. Investigative ophthalmology & visual science 2004; 45: 834–839

Garcia JPS, Garcia PT, Rosen RB. Retinal blood flow in the normal human eye using the canon laser blood flowmeter. Ophthalmic Research 2002; 34: 295–299

García-Antón MT, Salazar JJ, Hoz R de, Rojas B, Ramírez AI, Triviño A, Aroca-Aguilar J-D, García-Feijoo J, Escribano J, Ramírez JM. Goniodysgenesis variability and activity of CYP1B1 genotypes in primary congenital glaucoma. PloS One 2017; 12: e0176386

Garway-Heath DF, Poinoosawmy D, Fitzke FW, Hitchings RA. Mapping the visual field to the optic disc in normal tension glaucoma eyes. Ophthalmology 2000; 107: 1809–1815

Gedde SJ, Schiffman JC, Feuer WJ, Herndon LW, Brandt JD, Budenz DL. Treatment outcomes in the Tube Versus Trabeculectomy (TVT) study after five years of follow-up. American Journal of Ophthalmology 2012; 153: 789-803.e2

Gedde SJ, Vinod K, Wright MM, Muir KW, Lind JT, Chen PP, Li T, Mansberger SL, American Academy of Ophthalmology Preferred Practice Pattern Glaucoma Panel. Primary Open-Angle Glaucoma Preferred Practice Pattern®. Ophthalmology 2021; 128: P71-P150

Gillmann K, Rao HL, Mansouri K. Changes in peripapillary and macular vascular density after laser selective trabeculoplasty: an optical coherence tomography angiography study. Acta Ophthalmologica 2022; 100: 203–211

Gupta N, Ang L-C, Noël de Tilly L, Bidaisee L, Yücel YH. Human glaucoma and neural degeneration in intracranial optic nerve, lateral geniculate nucleus, and visual cortex. The British Journal of Ophthalmology 2006; 90: 674–678

Hamard P, Hamard H, Dufaux J, Quesnot S. Optic nerve head blood flow using a laser Doppler velocimeter and haemorheology in primary open angle glaucoma and normal pressure glaucoma. The British Journal of Ophthalmology 1994; 78: 449–453

Harris A, Rechtman E, Siesky B, Jonescu-Cuypers C, McCranor L, Garzozi HJ. The role of optic nerve blood flow in the pathogenesis of glaucoma. Ophthalmology clinics of North America 2005; 18: 345-53, v

Hayreh SS. Colour and fluorescence of the optic disc. Ophthalmologica. Journal international d'ophtalmologie. International journal of ophthalmology. Zeitschrift fur Augenheilkunde 1972; 165: 100–108

Heijl A, Leske MC, Bengtsson B, Hyman L, Bengtsson B, Hussein M, Early Manifest Glaucoma Trial Group. Reduction of intraocular pressure and glaucoma progression: results from the Early Manifest Glaucoma Trial. Archives of Ophthalmology (Chicago, Ill.: 1960) 2002; 120: 1268–1279

Ho CL, Walton DS. Primary congenital glaucoma: 2004 update. Journal of Pediatric Ophthalmology and Strabismus 2004; 41: 271-288; quiz 300-301

Holló G. Influence of Large Intraocular Pressure Reduction on Peripapillary OCT Vessel Density in Ocular Hypertensive and Glaucoma Eyes. Journal of glaucoma 2017; 26: e7-e10

Huang K-I, Su F-Y, Ho H-Y, Ho H-C, Chen Y-W, Lee C-K, Lai F, Lu HH-S, Ko M-L. Axial length, more than aging, decreases the thickness and superficial vessel density of retinal nerve fiber layer in non-glaucomatous eyes. International ophthalmology 2024; 44: 130

Hwang JC, Konduru R, Zhang X, Tan O, Francis BA, Varma R, Sehi M, Greenfield DS, Sadda SR, Huang D. Relationship among visual field, blood flow, and neural structure measurements in glaucoma. Investigative ophthalmology & visual science 2012; 53: 3020–3026

In JH, Lee SY, Cho SH, Hong YJ. Peripapillary Vessel Density Reversal after Trabeculectomy in Glaucoma. Journal of ophthalmology 2018; 2018: 8909714

Jayaram H, Kolko M, Friedman DS, Gazzard G. Glaucoma: now and beyond. The Lancet 2023; 402: 1788–1801

Jonas JB, Aung T, Bourne RR, Bron AM, Ritch R, Panda-Jonas S. Glaucoma. Lancet (London, England) 2017; 390: 2183–2193

Junoy Montolio FG, Müskens RPHM, Jansonius NM. Influence of glaucoma surgery on visual function: a clinical cohort study and meta-analysis. Acta Ophthalmologica 2019; 97: 193–199

Kashani AH, Chen C-L, Gahm JK, Zheng F, Richter GM, Rosenfeld PJ, Shi Y, Wang RK. Optical coherence tomography angiography: A comprehensive review of current methods and clinical applications. Progress in Retinal and Eye Research 2017; 60: 66–100

Keyser M de, Belder M de, Groot V de. Selective laser trabeculoplasty in pseudophakic and phakic eyes: a prospective study. International journal of ophthalmology 2017; 10: 593–598

Khodeiry M, Sayed MS. New glaucoma drainage implants available to glaucoma surgeons. Current Opinion in Ophthalmology 2023; 34: 176–180

Kim J-A, Kim T-W, Lee EJ, Girard MJA, Mari JM. Microvascular Changes in Peripapillary and Optic Nerve Head Tissues After Trabeculectomy in Primary Open-Angle Glaucoma. Investigative ophthalmology & visual science 2018; 59: 4614–4621

Kim Y-K, An Y, Park SP. INTRAOCULAR AND INTEROCULAR DIFFERENCES IN PARAFOVEAL VASCULAR DENSITY IN DIABETIC PATIENTS WITHOUT DIABETIC RETINOPATHY. Retina (Philadelphia, Pa.) 2021; 41: 170–180

Klugah-Brown B, Bore MC, Liu X, Gan X, Biswal BB, Kendrick KM, Chang DHF, Zhou B, Becker B. The neurostructural consequences of glaucoma and their overlap with disorders exhibiting emotional dysregulations: A voxel-based meta-analysis and tripartite system model. Journal of Affective Disorders 2024; 358: 487–499

Ko F, Papadopoulos M, Khaw PT. Primary congenital glaucoma. Progress in Brain Research 2015; 221: 177–189

Ko M-L, Peng P-H, Ma M-C, Ritch R, Chen C-F. Dynamic changes in reactive oxygen species and antioxidant levels in retinas in experimental glaucoma. Free Radical Biology & Medicine 2005; 39: 365–373

Koh V, Chew P, Triolo G, Lim KS, Barton K. Treatment Outcomes Using the PAUL Glaucoma Implant to Control Intraocular Pressure in Eyes with Refractory Glaucoma. Ophthalmology. Glaucoma 2020; 3: 350–359

Kook MS, Kim HB, Lee SU. Short-term effect of mitomycin-C augmented trabeculectomy on axial length and corneal astigmatism. Journal of cataract and refractive surgery 2001; 27: 518–523

Kourkoutas D, Buys YM, Flanagan JG, Karamaounas N, Georgopoulos G, Iliakis E, Moschos MM, Trope GE. Clinical significance of optic disc progression by topographic change analysis maps in glaucoma: an 8-year follow-up study. Journal of ophthalmology 2014; 2014: 987389

Kupfer C, Kaiser-Kupfer MI. Observations on the development of the anterior chamber angle with reference to the pathogenesis of congenital glaucomas. American Journal of Ophthalmology 1979; 88: 424–426

Labay-Tejado S, Ventura-Abreu N, Porto-Castro S, Castellarnau AD, Muniesa MJ, Millá E, Pazos M. Early safety and efficacy outcomes of the PAUL glaucoma implant in a Spanish population: A retrospective study. Saudi journal of ophthalmology : official journal of the Saudi Ophthalmological Society 2024; 38: 368–373

Lewis CJ, Hedberg-Buenz A, DeLuca AP, Stone EM, Alward WLM, Fingert JH. Primary congenital and developmental glaucomas. Human Molecular Genetics 2017; 26: R28-R36

Li L, Wang X, Liu C, Wang S, Wang X. Incidence Rate of Secondary Glaucoma Following Congenital Cataract Surgery: An In-Depth Systematic Review and Meta-Analysis. American Journal of Ophthalmology 2024; 265: 176–188

Lim R. The surgical management of glaucoma: A review. Clinical & experimental ophthalmology 2022; 50: 213–231

Lin Y-H, Huang S-M, Yeung L, Ku W-C, Chen HS-L, Lai C-C, Chuang L-H. Correlation of Visual Field With Peripapillary Vessel Density Through Optical Coherence Tomography Angiography in Normal-Tension Glaucoma. Translational vision science & technology 2020; 9: 26

Luntz MH. Congenital, infantile, and juvenile glaucoma. Ophthalmology 1979; 86: 793–802

Luo X, Shen Y-M, Jiang M-N, Lou X-F, Shen Y. Ocular Blood Flow Autoregulation Mechanisms and Methods. Journal of ophthalmology 2015; 2015: 864871

Mahmoudinezhad G, Moghimi S, Nishida T, Micheletti E, Du KH, Mohammadzadeh V, Wu J-H, Kamalipour A, Weinreb RN. Intraocular pressure increases the rate of macular vessel density loss in glaucoma. The British Journal of Ophthalmology 2024; 108: 181–187

Mannil SS, Agarwal A, Conner IP, Kumar RS. A comprehensive update on the use of optical coherence tomography angiography in glaucoma. International ophthalmology 2023; 43: 1785–1802

Maram J, Srinivas S, Sadda SR. Evaluating ocular blood flow. Indian Journal of Ophthalmology 2017; 65: 337–346

Matthiessen ET, Zeitz O, Richard G, Klemm M. Reproducibility of blood flow velocity measurements using colour decoded Doppler imaging. Eye (London, England) 2004; 18: 400–405

Mitchell P, Smith W, Chey T, Healey PR. Open-angle glaucoma and diabetes: the Blue Mountains eye study, Australia. Ophthalmology 1997; 104: 712–718

Moraes CG de, Liebmann JM, Greenfield DS, Gardiner SK, Ritch R, Krupin T. Risk factors for visual field progression in the low-pressure glaucoma treatment study. American Journal of Ophthalmology 2012; 154: 702–711

Musa I, Bansal S, Kaleem MA. Barriers to Care in the Treatment of Glaucoma: Socioeconomic Elements That Impact the Diagnosis, Treatment, and Outcomes in Glaucoma Patients. Current Ophthalmology Reports 2022; 10: 85–90

Nagar M, Luhishi E, Shah N. Intraocular pressure control and fluctuation: the effect of treatment with selective laser trabeculoplasty. The British Journal of Ophthalmology 2009; 93: 497–501

Nguyen H, Lee S-J, Li Y. Selective Activation of the Wnt-Signaling Pathway as a Novel Therapy for the Treatment of Diabetic Retinopathy and Other Retinal Vascular Diseases. Pharmaceutics 2022; 14

Nij Bijvank J, Maillette de Buy Wenniger L, Graaf P de, Petzold A. Clinical review of retinotopy. The British Journal of Ophthalmology 2023; 107: 304–312

Nouri-Mahdavi K, Brigatti L, Weitzman M, Caprioli J. Outcomes of trabeculectomy for primary open-angle glaucoma. Ophthalmology 1995; 102: 1760–1769

Nuzzi R, Dallorto L, Rolle T. Changes of Visual Pathway and Brain Connectivity in Glaucoma: A Systematic Review. Frontiers in Neuroscience 2018; 12

Oatts JT, Han Y. Glaucoma Drainage Device Implantation, Outcomes, and Complications. International ophthalmology clinics 2023; 63: 93–101

Olafsdottir OB, Vandewalle E, Abegão Pinto L, Geirsdottir A, Clerck E de, Stalmans P, Gottfredsdottir MS, Kristjansdottir JV, van Calster J, Zeyen T, Stefánsson E, Stalmans I. Retinal oxygen metabolism in healthy subjects and glaucoma patients. The British Journal of Ophthalmology 2014; 98: 329–333

Pakravan M, Homayoon N, Shahin Y, Ali Reza BR. Trabeculectomy with mitomycin C versus Ahmed glaucoma implant with mitomycin C for treatment of pediatric aphakic glaucoma. Journal of glaucoma 2007; 16: 631–636

Park H-YL, Hong KE, Da Shin Y, Jung Y, Kim EK, Park CK. Microvasculature Recovery Detected Using Optical Coherence Tomography Angiography and the Rate of Visual Field Progression After Glaucoma Surgery. Investigative ophthalmology & visual science 2021; 62: 17

Patel N, McAllister F, Pardon L, Harwerth R. The effects of graded intraocular pressure challenge on the optic nerve head. Experimental eye research 2018; 169: 79–90

Pillunat LE, Stodtmeister R, Wilmanns I. Pressure compliance of the optic nerve head in low tension glaucoma. The British Journal of Ophthalmology 1987; 71: 181–187

Poelman HJ, Wolfs RCW, Ramdas WD. The Baerveldt Glaucoma Drainage Device: Efficacy, Safety, and Place in Therapy. Clinical Ophthalmology (Auckland, N.Z.) 2020; 14: 2789–2797

Pollack A, Marcovich A, Bukelman A, Oliver M. Age-related macular degeneration after extracapsular cataract extraction with intraocular lens implantation. Ophthalmology 1996; 103: 1546–1554

Quigley HA, Addicks EM. Chronic experimental glaucoma in primates. II. Effect of extended intraocular pressure elevation on optic nerve head and axonal transport. Investigative ophthalmology & visual science 1980; 19: 137–152

Quigley HA, Addicks EM, Green WR, Maumenee AE. Optic nerve damage in human glaucoma. II. The site of injury and susceptibility to damage. Archives of Ophthalmology (Chicago, Ill.: 1960) 1981; 99: 635–649

Raghu N, Pandav SS, Kaushik S, Ichhpujani P, Gupta A. Effect of trabeculectomy on RNFL thickness and optic disc parameters using optical coherence tomography. Eye 2012; 26: 1131–1137

Ramdas WD, Pals J, Rothova A, Wolfs RCW. Efficacy of glaucoma drainage devices in uveitic glaucoma and a meta-analysis of the literature. Graefe’s Archive for Clinical and Experimental Ophthalmology = Albrecht Von Graefes Archiv Fur Klinische Und Experimentelle Ophthalmologie 2019; 257: 143–151

Rankin SJ, Drance SM, Buckley AR, Walman BE. Visual field correlations with color Doppler studies in open angle glaucoma. Journal of glaucoma 1996; 5: 15–21

Reber F, Gersch U, Funk RW. Blockers of carbonic anhydrase can cause increase of retinal capillary diameter, decrease of extracellular and increase of intracellular pH in rat retinal organ culture. Graefe's archive for clinical and experimental ophthalmology = Albrecht von Graefes Archiv fur klinische und experimentelle Ophthalmologie 2003; 241: 140–148

Resch H, Schmidl D, Hommer A, Rensch F, Jonas JB, Fuchsjäger-Mayrl G, Garhöfer G, Vass C, Schmetterer L. Correlation of optic disc morphology and ocular perfusion parameters in patients with primary open angle glaucoma. Acta Ophthalmologica 2011; 89: e544-9

Resch MD, Balogh A, Lászik G, Nagy ZZ, Papp A. Association between retinal vessel density and postoperative time after primary repair of rhegmatogenous retinal detachment. PloS One 2021; 16: e0258126

Sampson DM, Gong P, Di An, Menghini M, Hansen A, Mackey DA, Sampson DD, Chen FK. Axial Length Variation Impacts on Superficial Retinal Vessel Density and Foveal Avascular Zone Area Measurements Using Optical Coherence Tomography Angiography. Investigative ophthalmology & visual science 2017; 58: 3065–3072

Schargus M, Theilig T, Rehak M, Busch C, Bormann C, Unterlauft JD. Outcome of a single XEN microstent implant for glaucoma patients with different types of glaucoma. BMC ophthalmology 2020; 20: 490

Sehi M. Basic technique and anatomically imposed limitations of confocal scanning laser Doppler flowmetry at the optic nerve head level. Acta Ophthalmologica 2011; 89: e1-11

Shiga Y, Kunikata H, Aizawa N, Kiyota N, Maiya Y, Yokoyama Y, Omodaka K, Takahashi H, Yasui T, Kato K, Iwase A, Nakazawa T. Optic Nerve Head Blood Flow, as Measured by Laser Speckle Flowgraphy, Is Significantly Reduced in Preperimetric Glaucoma. Current Eye Research 2016; 41: 1447–1453

Shiga Y, Omodaka K, Kunikata H, Ryu M, Yokoyama Y, Tsuda S, Asano T, Maekawa S, Maruyama K, Nakazawa T. Waveform analysis of ocular blood flow and the early detection of normal tension glaucoma. Investigative ophthalmology & visual science 2013; 54: 7699–7706

Shin JW, Sung KR, Uhm KB, Jo J, Moon Y, Song MK, Song JY. Peripapillary Microvascular Improvement and Lamina Cribrosa Depth Reduction After Trabeculectomy in Primary Open-Angle Glaucoma. Investigative ophthalmology & visual science 2017; 58: 5993–5999

Shoji T, Kanno J, Weinreb RN, Yoshikawa Y, Mine I, Ishii H, Ibuki H, Shinoda K. OCT angiography measured changes in the foveal avascular zone area after glaucoma surgery. The British Journal of Ophthalmology 2022; 106: 80–86

Siesky B, Harris A, Brizendine E, Marques C, Loh J, Mackey J, Overton J, Netland P. Literature review and meta-analysis of topical carbonic anhydrase inhibitors and ocular blood flow. Survey of Ophthalmology 2009; 54: 33–46

Sigal IA, Ethier CR. Biomechanics of the optic nerve head. Experimental eye research 2009; 88: 799–807

Sihota R, Mahalingam K, Maurya AK, Sharma A, Bukke AN, Dada T. Primary congenital glaucoma: An iridotrabeculodysgenesis? Indian Journal of Ophthalmology 2024; 72: 328–334

Song S, Yu X, Zhang P, Dai H. Changes in Macular Microvascular Structure in Macular Edema Secondary to Branch Retinal Vein Occlusion Treated with Antivascular Endothelial Growth Factor for One Year. Journal of ophthalmology 2021; 2021: 6645452

Spaide RF, Fujimoto JG, Waheed NK, Sadda SR, Staurenghi G. Optical coherence tomography angiography. Progress in Retinal and Eye Research 2018; 64: 1–55

Stallworth JY, O'Brien KS, Han Y, Oatts JT. Efficacy of Ahmed and Baerveldt glaucoma drainage device implantation in the pediatric population: A systematic review and meta-analysis. Survey of Ophthalmology 2023; 68: 578–590

Staurenghi G, Viola F, Mainster MA, Graham RD, Harrington PG. Scanning laser ophthalmoscopy and angiography with a wide-field contact lens system. Archives of Ophthalmology (Chicago, Ill.: 1960) 2005; 123: 244–252

Stein JD, Khawaja AP, Weizer JS. Glaucoma in Adults-Screening, Diagnosis, and Management: A Review. JAMA 2021; 325: 164–174

Sun X, Dai Y, Chen Y, Yu D-Y, Cringle SJ, Chen J, Kong X, Wang X, Jiang C. Primary angle closure glaucoma: What we know and what we don’t know. Progress in Retinal and Eye Research 2017; 57: 26–45

Tan MCJ, Ong CW, Aquino MC, Lun KW, Sng CCA, Lim DKA, Loon SC, Koh VTC, Chew PTK. Three-Year Outcomes of the Paul Glaucoma Implant for Treatment of Glaucoma. Journal of glaucoma 2024; 33: 478

Tang Y, Shi Y, Fan Z. The mechanism and therapeutic strategies for neovascular glaucoma secondary to diabetic retinopathy. Frontiers in Endocrinology 2023; 14: 1102361

Tezel G. Oxidative stress in glaucomatous neurodegeneration: mechanisms and consequences. Progress in Retinal and Eye Research 2006; 25: 490–513

Tham Y-C, Li X, Wong TY, Quigley HA, Aung T, Cheng C-Y. Global prevalence of glaucoma and projections of glaucoma burden through 2040: a systematic review and meta-analysis. Ophthalmology 2014; 121: 2081–2090

Thomas S, Hodge W, Malvankar-Mehta M. The Cost-Effectiveness Analysis of Teleglaucoma Screening Device. PloS One 2015; 10: e0137913

Tsuda S, Yokoyama Y, Chiba N, Aizawa N, Shiga Y, Yasuda M, Yokokura S, Otomo T, Fuse N, Nakazawa T. Effect of topical tafluprost on optic nerve head blood flow in patients with myopic disc type. Journal of glaucoma 2013; 22: 398–403

Vallabh NA, Mohindra R, Drysdale E, Mason F, Fenerty CH, Yau K. The PAUL® glaucoma implant: 1-year results of a novel glaucoma drainage device in a paediatric cohort. Graefe's Archive for Clinical and Experimental Ophthalmology = Albrecht Von Graefes Archiv Fur Klinische Und Experimentelle Ophthalmologie 2023; 261: 2351–2358

van Koolwijk LME, Ramdas WD, Ikram MK, Jansonius NM, Pasutto F, Hysi PG, Macgregor S, Janssen SF, Hewitt AW, Viswanathan AC, Brink JB ten, Hosseini SM, Amin N, Despriet DDG, Willemse-Assink JJM, Kramer R, Rivadeneira F, Struchalin M, Aulchenko YS, Weisschuh N, Zenkel M, Mardin CY, Gramer E, Welge-Lüssen U, Montgomery GW, Carbonaro F, Young TL, Bellenguez C, McGuffin P, Foster PJ, Topouzis F, Mitchell P, Wang JJ, Wong TY, Czudowska MA, Hofman A, Uitterlinden AG, Wolfs RCW, Jong PTVM de, Oostra BA, Paterson AD, Mackey DA, Bergen AAB, Reis A, Hammond CJ, Vingerling JR, Lemij HG, Klaver CCW, van Duijn CM. Common

Genetic Determinants of Intraocular Pressure and Primary Open-Angle Glaucoma. PLoS Genetics 2012; 8: e1002611

Verticchio Vercellin AC, Harris A, Oddone F, Siesky B, Eckert G, Belamkar A, Antman G, Segev F. Ocular blood flow biomarkers may predict long-term glaucoma progression. The British Journal of Ophthalmology 2024; 108: 946–950

Vries MM de, Müskens RPHM, Renardel de Lavalette VW, Hooymans JMM, Jansonius NM. Glaucoma drainage device surgery after vitreoretinal surgery: incidence and risk factors. Acta Ophthalmologica 2016; 94: 135–139

Wagner FM, Schuster AK-G, Emmerich J, Chronopoulos P, Hoffmann EM. Efficacy and safety of XEN®-Implantation vs. trabeculectomy: Data of a "real-world" setting. PloS One 2020; 15: e0231614

Walkden A, Au L. Iridocorneal endothelial syndrome: clinical perspectives. Clinical Ophthalmology (Auckland, N.Z.) 2018; 12: 657–664

Wang L, Cull G, Burgoyne CF, Thompson S, Fortune B. Longitudinal alterations in the dynamic autoregulation of optic nerve head blood flow revealed in experimental glaucoma. Investigative ophthalmology & visual science 2014; 55: 3509–3516

Wang X, Chen J, Kong X, Sun X. Immediate Changes in Peripapillary Retinal Vasculature after Intraocular Pressure Elevation -an Optical Coherence Tomography Angiography Study. Current Eye Research 2020; 45: 749–756

Weber C, Hundertmark S, Liegl R, Jauch AS, Stasik I, Holz FG, Mercieca K. Clinical outcomes of the PAUL® glaucoma implant: One-year results. Clinical & experimental ophthalmology 2023; 51: 566–576

Weber C, Hundertmark S, Stasik I, Holz FG, Mercieca K. Two-Year Clinical Outcomes of the PAUL Glaucoma Implant in White Patients With Refractory Glaucoma. Journal of glaucoma 2024; 33: 808–814

Weigert G, Findl O, Luksch A, Rainer G, Kiss B, Vass C, Schmetterer L. Effects of moderate changes in intraocular pressure on ocular hemodynamics in patients with

primary open-angle glaucoma and healthy controls. Ophthalmology 2005; 112: 1337–1342

Weinreb RN, Khaw PT. Primary open-angle glaucoma. Lancet (London, England) 2004; 363: 1711–1720

Weinreb RN, Leung CKS, Crowston JG, Medeiros FA, Friedman DS, Wiggs JL, Martin KR. Primary open-angle glaucoma. Nature Reviews. Disease Primers 2016; 2: 16067

Wiggs JL, Pasquale LR. Genetics of glaucoma. Human Molecular Genetics 2017; 26: R21-R27

Williams AL, Eason J, Chawla B, Bohnsack BL. Cyp1b1 Regulates Ocular Fissure Closure Through a Retinoic Acid-Independent Pathway. Investigative ophthalmology & visual science 2017; 58: 1084–1097

Wright WS, Eshaq RS, Lee M, Kaur G, Harris NR. Retinal Physiology and Circulation: Effect of Diabetes. Comprehensive Physiology 2020; 10: 933–974

Yarmohammadi A, Zangwill LM, Diniz-Filho A, Suh MH, Yousefi S, Saunders LJ, Belghith A, Manalastas PIC, Medeiros FA, Weinreb RN. Relationship between Optical Coherence Tomography Angiography Vessel Density and Severity of Visual Field Loss in Glaucoma. Ophthalmology 2016; 123: 2498–2508

Yuan Y, Dong M, Wen S, Yuan X, Zhou L. Retinal microcirculation: A window into systemic circulation and metabolic disease. Experimental eye research 2024; 242: 109885

Zéboulon P, Lévêque P-M, Brasnu E, Aragno V, Hamard P, Baudouin C, Labbé A. Effect of Surgical Intraocular Pressure Lowering on Peripapillary and Macular Vessel Density in Glaucoma Patients: An Optical Coherence Tomography Angiography Study. Journal of glaucoma 2017; 26: 466–472

Zhang N, Wang J, Li Y, Jiang B. Prevalence of primary open angle glaucoma in the last 20 years: a meta-analysis and systematic review. Scientific Reports 2021; 11: 13762

Zhong H, Dong Q, Cun Q, He G, Tao Y, Song K, Lu Y, Zhu Q, Chen X, Chen Q. Peripapillary vessel density correlates with visual field mean sensitivity in highly myopic eyes. Journal of translational medicine 2022; 20: 119

Zukerman R, Harris A, Vercellin AV, Siesky B, Pasquale LR, Ciulla TA. Molecular Genetics of Glaucoma: Subtype and Ethnicity Considerations. Genes 2020; 12: 55

# 9 Statement on personal contributions

The work was carried out at the Eye clinic of University Hospital of Bonn under the supervision of Prof. Dr. med. Frank G. Holz and Dr. Karl Mercieca.

The concept of the study was developed in collaboration with Dr. Karl Mercieca.

The following experiments were carried out by me with support from Ms. Ke Lu.

The data material used for the analysis was independently generated by me.

The statistical analysis was carried out independently by me.

While preparing this work, I used ChatGPT (GPT-4o) to improve the readability and language of the thesis. After using this tool, I reviewed and edited the corresponding paragraphs as needed and take full responsibility for the content of the published doctoral thesis. Additional details if applicable.

I confirm that I have written this doctoral thesis independently and that I have listed all sources and resources used.

## 10 Acknowledgments

I would like to express my sincere gratitude to Dr. Karl Mercieca for his invaluable guidance, continuous support, and insightful feedback throughout my doctoral studies. I am deeply grateful to my family for their support and understanding over the past years. Lastly, I thank myself for making it through this journey.